All-dielectric metasurfaces with full phase control by using only electric response

Grigorii Ptitcyn

School of Science

Thesis submitted for examination for the degree of Master of Science (Technology).
Espoo 18.9.2017

Thesis supervisor:

Prof. Sergei A. Tretyakov

Thesis instructor:

Ph.D. Ana Díaz-Rubio

Aalto University
School of Science

AALTO UNIVERSITY
School of Science
Master's Programme in Engineering Physics

ABSTRACT OF THE
MASTER'S THESIS

Author: Grigorii Ptitcyn

Title: All-dielectric metasurfaces with full phase control by using only electric response

Date: 18.9.2017 Language: English Number of pages: 7+48

Major or Minor: Radio Science and Engineering

Supervisor: Prof. Sergei A. Tretyakov

Instructor: Ph.D. Ana Díaz-Rubio

This thesis studies different approaches for designing transmitting metasurfaces. The goal was to develop a novel approach that enables full phase control of the transmitted field. The suggested method utilizes metasurfaces at oblique incidence, which enables excitation of additional resonating modes. Spectrally overlapped electric eigenmodes give 2π phase coverage with high transmission amplitude. This approach is used in order to create a transmitarray, which refracts incident light at a desired angle. The results show that the suggested approach can be used to design robust and low-loss metasurfaces.

Keywords: Metasurfaces, all-dielectric, optics, full phase control, transmitarray.

Preface

This thesis was made in Aalto University School of Electrical Engineering at the Department of Electronics and Nanoengineering in the research group of Theoretical and Applied Electromagnetics of Complex Media in 2017. I would like to thank my supervisor Prof. Sergei A. Tretyakov for his wise and coherent guidance and for the possibility to work on such exciting topic. I also thank my instructor Ph.D. Ana Diaz-Rubio and others who have guided me during the past year, especially, Viktar Asadchy.

Finally, I would like to thank my family for giving me a chance to study abroad and for supporting me during my studies.

Otaniemi, 18.9.2017

Grigorii Ptitcyn

Contents

Symbols

$\mathbf{E}$	electric field vector
$\mathbf{H}$	magnetic field vector
μ	permeability
ε	permittivity
$\mathbf{M}$	magnetic polarization density
$\mathbf{P}$	electric polarization density
ω	angular frequency
δ	Dirac delta function
$\mathbf{E}_t$	tangential component of electric field
$\mathbf{H}_t$	tangential component of magnetic field
E_n	normal component of electric field
H_n	normal component of magnetic field
$\mathbf{n}$	unit vector defining the normal to the surface
$\mathbf{M}_t$	tangential component of the magnetic polarization density
$\mathbf{P}_t$	tangential component of the electric polarization density
M_n	normal component of the magnetic polarization density
P_n	normal component of the electric polarization density
∇	nabla operator
∇_t	tangential component of nabla operator
$\mathbf{x}_0$, $\mathbf{y}_0$, $\mathbf{z}_0$	unit vectors of the cartesian coordinate system
$\mathbf{E}_t^+$	tangential component of electric field above the metasurface
$\mathbf{E}_t^-$	tangential component of electric field below the metasurface
$\mathbf{H}_t^+$	tangential component of magnetic field above the metasurface
$\mathbf{H}_t^-$	tangential component of magnetic field below the metasurface
$\mathbf{p}$	electric dipole moment
$\mathbf{m}$	magnetic dipole moment
S	area of the supercell

$\hat{\bar{\alpha}}^{\mathrm{ee}}$	electric collective polarizability tensor
$\hat{\bar{\alpha}}^{\mathrm{em}}$	electro-magnetic collective polarizability tensor
$\hat{\bar{\alpha}}^{\mathrm{me}}$	magneto-electric collective polarizability tensor
$\hat{\bar{\alpha}}^{\mathrm{mm}}$	magnetic collective polarizability tensor
$\mathbf{E}_{\mathrm{i}}$	incident electric field
$\mathbf{H}_{\mathrm{i}}$	incident magnetic field
$\hat{\bar{\chi}}^{\mathrm{ee}}$	electric collective susceptibility tensor
$\hat{\bar{\chi}}^{\mathrm{em}}$	electro-magnetic collective susceptibility tensor
$\hat{\bar{\chi}}^{\mathrm{me}}$	magneto-electric collective susceptibility tensor
$\hat{\bar{\chi}}^{\mathrm{mm}}$	magnetic collective susceptibility tensor
$\mathbf{E}_{\mathrm{ave}}$	averaged electric field
$\mathbf{H}_{\mathrm{ave}}$	averaged magnetic field
$\bar{\bar{A}}$, $\bar{\bar{B}}$, $\bar{\bar{C}}$, $\bar{\bar{D}}$	coefficients of the $ABCD$-matrix
Z_{ij}	Z-parameters
θ_{i}	angle of incidence
θ_{t}	angle of transmission
$\eta_{1,2}$	impedances of the first and second media
$k_{1,2}$	wavenumbers in the the first and second media
E_{i}	amplitude of the incident field
E_{t}	amplitude of the transmitted field
T	local transmission coefficient
ϕ_{t}	local phase shift of the transmitted field
Φ_{t}	phase shift along the metasurface
D	size of the supercell
S_{ij}	scattering parameters
η_0	free space impedance
Z_{in}	input impedance
Z_{out}	output impedance
R	local reflection coefficient

P_{in}	input power
P_{out}	output power
ξ	efficiency
w	width of the bars
h	height of the bars
n_{d}	refractive index of the dielectric material
n_{sub}	refractive index of the substrate

1 Introduction

Modern electronics, radio and microwave techniques demonstrate impressive results in miniaturization, integration, efficiency and speed. Recent technologies allow to manufacture devices that are miniature not only in practical terms, but also small in comparison to the wavelength of the radiation they can control. However, the miniaturization of modern electronic devices is approaching the limit imposed by nature. In order to push this limit further, other techniques have to be developed. Currently, photonic devices represent the most promising solution for this problem. At present, only transmission of signals to long distances is performed optically. Processing of signals and computations are done electronically. The performance of telecommunication systems, based on conducting wires, is fundamentally limited by two factors. One is the thermal noise. In the microwave and radio frequency regions it is a serious problem, whereas in the optical domain the thermal noise level is practically negligible. The other limitation is imposed by the dispersion and power loss in electronic interconnects. Inevitable losses in metal conductors lead to signal propagation loss and device heating. Dispersion causes distortion of signals and information loss. In optics, free-space propagation is dispersion free. Therefore, all such problems can be solved by using the optical devices. However, the conventional optical devices are bulky, and existing technologies do not allows integration of many functions in a single device which would be as compact as its electronic analogue. Nevertheless, the necessary condition of a significant breakthrough in telecommunications is replacement of electronic devices with compact optical ones.

In order to use photons instead of electrons, optical devices of the future should allow complete control over light. However, currently available materials do not possess the necessary properties. The performance of natural materials is limited, because their electromagnetic properties are determined by the chemical composition of atoms and molecules. Usually, light-matter interactions are described in terms of the material parameters: permittivity (ε) and permeability (μ). In the optical frequency range, these parameters vary in a quite narrow range. Therefore, for

realizing optical devices, the range of available properties has to be extended. For this purpose a concept of metamaterials can be used. Usually, metamaterials are defined as materials whose electromagnetic properties are determined by their artificial structure instead of the properties of the materials they are made of [1, 2]. Ordinary materials are made of atoms, whereas metamaterials are made of "meta-atoms". Electromagnetic properties of metamaterials are governed not only by the shape and periodicity of the meta-atoms, but also by their mutual positions and orientations in the composite materials. The size of meta-atoms is far larger than that of ordinary atoms, however it has to be sufficiently small on the wavelength scale of interest.

Modern nano fabrication techniques allow creation of small meta-atoms even for the optical range. However, implementation of bulk periodical arrays is quite difficult, especially in the optical domain. Inevitable losses due to their resonant behavior, in addition to the propagation losses, can diminish or even destroy the performance of the devices. Therefore, a concept of metasurfaces can be used to solve these problems. Metasurfaces are arrangements of meta-atoms on a surface. They are also defined as two-dimensional metamaterials. Metasurfaces are much easier to fabricate in comparison to bulk metamaterials and, despite the very small thickness, they are able to cause a significant effect on the incident field. In addition to that, metasurfaces can be easily integrated into miniature devices, due to their thin profile. All these reasons have made metasurfaces widely studied over the last decade.

The goal of this thesis is to study a new approach of achieving full phase control of wave passing a metasurface. This is essential for realizing many devices, such as reflectarrays, lenses and holograms, however in this thesis a transmitarray will be designed. The phase change on the surface of such device is set to transmit incident light at a desired angle. The design of the transmitarray is presented only for demonstration of the phenomenon. Whereas, the main focus is on obtaining full phase control by using only electric response of the metasurface. The approach is utilized in the simulations of the designed transmitarray. The results show that the suggested approach enables full phase coverage, therefore, it can be used in various

metasurface designs.

The structure of the thesis is as follows: After the introduction, a literature review is presented. On the basis of previous studies different approaches for characterization of metasurfaces are considered. The first approach considers a metasurface inside thin dielectric layer, in order to derive the generalized sheet transition conditions. Another approach considers a metasurface in terms of the circuit theory. In Section 3, utilization of this theory allowed us to simulate transmitarrays. This section also reviews practical realization of metasurfaces in microwaves and in optics. In Section 4 a metasurface is considered at normal and oblique incidences. Full phase control for normal incidence was achieved in previous works, by overlapping magnetic and electric resonances. However, the scientifically new approach introduced in this section allows to obtain full phase control by using only electric response. In Section 5 this approach is implemented for realizing transmitarrays in the optical region.

2 Characterization of metasurfaces, literature overview

2.1 Generalized sheet boundary conditions

By definition, the thickness of a metasurface is small in comparison to the wavelength. Nevertheless, it may cause a significant change of the fields. In order to describe this change, it is possible to write transition conditions through a thin layer. The derivation of the generalized sheet transition conditions, performed in this section, is based on Refs. [1, 3]. Let us consider a metasurface inside a dielectric slab, which in turn is located in free space. The dielectric slab is characterized by thickness d, permittivity ε and permeability μ. In this case, the thickness d is assumed to be negligible compared to the wavelength inside the slab's material. A schematic representation of the problem is shown in Fig. 1.

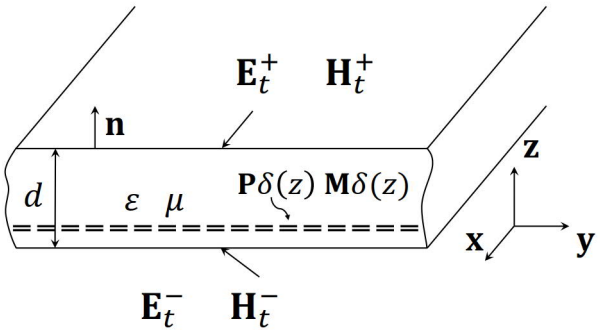

Figure 1: Geometry of the problem with a thin dielectric layer.

Without loosing generality, it is possible to assume that the slab lies in the xy plane. The electric and magnetic fields ($\mathbf{E}$ and $\mathbf{H}$) inside the slab are described by Maxwell equations, that can be specified as

$$\nabla \times \mathbf{E} = -j\omega\mu\left(\mathbf{H} + \frac{\mathbf{M}\delta(z)}{\mu}\right), \quad \nabla \times \mathbf{H} = j\omega\varepsilon\left(\mathbf{E} + \frac{\mathbf{P}\delta(z)}{\varepsilon}\right), \tag{1}$$

where $\mathbf{P}$ and $\mathbf{M}$ are electric and magnetic polarizations of the metasurface. Frequency of the incident wave in free space is ω. In the derivation time-harmonic dependency,

$e^{j\omega t}$, is assumed. Considering normal (E_n and H_n) and tangential ($\mathbf{E}_t$ and $\mathbf{H}_t$) components separately allows to split the equations. Therefore, field vectors can be rewritten, by using vector $\mathbf{n}$, which is normal to the slab,

$$\mathbf{E} = \mathbf{E}_\mathrm{t} + \mathbf{n}E_\mathrm{n}, \quad \mathbf{H} = \mathbf{H}_\mathrm{t} + \mathbf{n}H_\mathrm{n}, \tag{2}$$

where

$$\mathbf{E}_\mathrm{t} \cdot \mathbf{n} = 0, \quad \mathbf{H}_\mathrm{t} \cdot \mathbf{n} = 0. \tag{3}$$

By following the same procedure polarizations $\mathbf{P}$ and $\mathbf{M}$ can be decomposed in a similar way:

$$\mathbf{P} = \mathbf{P}_\mathrm{t} + \mathbf{n}P_\mathrm{n}, \quad \mathbf{M} = \mathbf{M}_\mathrm{t} + \mathbf{n}M_\mathrm{n}, \tag{4}$$

where

$$\mathbf{P}_\mathrm{t} \cdot \mathbf{n} = 0, \quad \mathbf{M}_\mathrm{t} \cdot \mathbf{n} = 0. \tag{5}$$

Operator ∇ can be expressed thorough the tangential and normal components as well,

$$\nabla = \underbrace{\frac{\partial}{\partial x}\mathbf{x_0} + \frac{\partial}{\partial y}\mathbf{y_0}}_{\nabla_\mathrm{t}} + \frac{\partial}{\partial z}\mathbf{z_0} = \nabla_\mathrm{t} + \frac{\partial}{\partial z}\mathbf{z_0}. \tag{6}$$

Finally, equations in (1) can be divided into two sets of equations with tangential components of the polarizations,

$$\begin{aligned} \nabla_\mathrm{t} \times \mathbf{n}E_\mathrm{n} + \frac{\partial}{\partial z}(\mathbf{n} \times \mathbf{E}_\mathrm{t}) &= -j\omega\mu\mathbf{H}_\mathrm{t} - j\omega\mathbf{M}_\mathrm{t}\delta(z), \\ \nabla_\mathrm{t} \times \mathbf{n}H_\mathrm{n} + \frac{\partial}{\partial z}(\mathbf{n} \times \mathbf{H}_\mathrm{t}) &= j\omega\varepsilon\mathbf{E}_\mathrm{t} + j\omega\mathbf{P}_\mathrm{t}\delta(z), \end{aligned} \tag{7}$$

and with their normal components,

$$\begin{aligned} \mathbf{n}E_\mathrm{n} &= -\frac{1}{j\omega\varepsilon}\nabla_\mathrm{t} \times \mathbf{H}_\mathrm{t} - \mathbf{n}\frac{P_\mathrm{n}\delta(z)}{\varepsilon}, \\ \mathbf{n}H_\mathrm{n} &= \frac{1}{j\omega\mu}\nabla_\mathrm{t} \times \mathbf{E}_\mathrm{t} - \mathbf{n}\frac{M_\mathrm{n}\delta(z)}{\mu}. \end{aligned} \tag{8}$$

Next, the initial equations in (1) can be rewritten in terms of only the tangential components. By substituting equations in (8) into (7) the result reads:

$$\frac{\partial}{\partial z}\mathbf{n}\times\mathbf{E}_{\mathrm{t}} = -j\omega\mu\mathbf{H}_{\mathrm{t}} - \frac{1}{j\omega\varepsilon}\nabla_{\mathrm{t}}\times\nabla_t\times\mathbf{H}_{\mathrm{t}} - j\omega\mathbf{M}_{\mathrm{t}}\delta(z) + \nabla_{\mathrm{t}}\times\mathbf{n}\frac{P_{\mathrm{n}}\delta(z)}{\varepsilon}, \tag{9}$$

$$\frac{\partial}{\partial z}\mathbf{n}\times\mathbf{H}_{\mathrm{t}} = j\omega\varepsilon\mathbf{E}_{\mathrm{t}} + \frac{1}{j\omega\mu}\nabla_{\mathrm{t}}\times\nabla_{\mathrm{t}}\times\mathbf{E}_{\mathrm{t}} + j\omega\mathbf{P}_{\mathrm{t}}\delta(z) + \nabla_{\mathrm{t}}\times\mathbf{n}\frac{M_{\mathrm{n}}\delta(z)}{\mu}. \tag{10}$$

By integrating both these equations over the thickness of the slab d and assuming that the metasurface is infinitely thin, a limit $d\to 0$ can be taken. Integrals of the tangential field components are zero, because the surface averaged fields are finite, but the integration interval d tends to zero. Therefore, the only survived components contained delta-functions. Equation (9) is cross-multiplied by $\mathbf{n}$ and it results in the following set of generalized sheet transition conditions [3–6]:

$$\mathbf{E}_{\mathrm{t}}^{+} - \mathbf{E}_{\mathrm{t}}^{-} = j\omega\mathbf{n}\times\mathbf{M}_{\mathrm{t}} - \nabla_{\mathrm{t}}\frac{P_{\mathrm{n}}}{\varepsilon}, \tag{11}$$

$$\mathbf{n}\times\mathbf{H}_{\mathrm{t}}^{+} - \mathbf{n}\times\mathbf{H}_{\mathrm{t}}^{-} = j\omega\mathbf{P}_{\mathrm{t}} - \nabla_{\mathrm{t}}\times\mathbf{n}\frac{M_{\mathrm{n}}}{\mu}, \tag{12}$$

where subscript t refers to the tangential field components and superscripts $+$ and $-$ denote field components above and below the metasurface. These equations relate jumps of the tangential components of electric and magnetic fields across the sheet due to the surface electric and magnetic polarizations.

At the same time, electric and magnetic dipole moments ($\mathbf{p}$ and $\mathbf{m}$) can be expressed through the electromagnetic fields ($\mathbf{E}$ and $\mathbf{H}$). The parameters that relate the incident fields with the dipole moments are called polarizabilities. They do not depend on the conditions of the external excitation. The polarizabilities characterize the metasurface itself and they depend only on the physical parameters of the metasurface. Therefore, in the general case the polarizabilities are tensors. Relations between the incident field and the dipole moments read:

$$\begin{aligned}\mathbf{p} &= \hat{\bar{\alpha}}^{\mathrm{ee}}\cdot\mathbf{E}_{\mathrm{i}} + \hat{\bar{\alpha}}^{\mathrm{em}}\cdot\mathbf{H}_{\mathrm{i}},\\ \mathbf{m} &= \hat{\bar{\alpha}}^{\mathrm{me}}\cdot\mathbf{E}_{\mathrm{i}} + \hat{\bar{\alpha}}^{\mathrm{mm}}\cdot\mathbf{H}_{\mathrm{i}},\end{aligned} \tag{13}$$

where collective polarizabilities $\hat{\bar{\alpha}}^{\mathrm{ee}}$, $\hat{\bar{\alpha}}^{\mathrm{em}}$, $\hat{\bar{\alpha}}^{\mathrm{me}}$, $\hat{\bar{\alpha}}^{\mathrm{mm}}$ are called electric, magnetoelectric, electromagnetic and magnetic polarizabilities, respectively. The polarization density

vectors equal $\mathbf{P} = \mathbf{p}/S$, $\mathbf{M} = \mathbf{m}/S$, where S is the unit cell area. Another approach relates averaged fields with the polarizations, by using susceptibility tensors $\hat{\hat{\chi}}$. The averaged fields can be introduced as

$$\begin{aligned} \mathbf{E}^{\text{ave}} &= \frac{\mathbf{E}_{\text{i}} + \mathbf{E}_{\text{r}} + \mathbf{E}_{\text{t}}}{2}, \\ \mathbf{H}^{\text{ave}} &= \frac{\mathbf{H}_{\text{i}} + \mathbf{H}_{\text{r}} + \mathbf{H}_{\text{t}}}{2}, \end{aligned} \tag{14}$$

where subscripts i, r and t refer to the incident, reflected and transmitted wave fields, respectively. By expressing polarizations through the averaged fields, the result reads:

$$\begin{aligned} \mathbf{P} &= \hat{\hat{\chi}}^{\text{ee}} \cdot \mathbf{E}_{\text{ave}} + \hat{\hat{\chi}}^{\text{em}} \cdot \mathbf{H}_{\text{ave}}, \\ \mathbf{M} &= \hat{\hat{\chi}}^{\text{me}} \cdot \mathbf{E}_{\text{ave}} + \hat{\hat{\chi}}^{\text{mm}} \cdot \mathbf{H}_{\text{ave}}. \end{aligned} \tag{15}$$

Both the polarizabilities and susceptibilities can be retrieved from the measurements by using the reflection and transmission coefficients. An alternative approach based on surface impedance tensor can be used for modelling the metasurface, allowing its interpretation through an equivalent circuit. This method will be discussed in the following section.

2.2 Equivalent circuit interpretation of metasurfaces

One of the possible ways to describe a metasurface response is to model it by using impedance matrices. In this case it might be useful to consider a metasurface in terms of the theory introduce in Refs. [1,7]. This approach considers a metasurface in terms of the circuit theory. The electric and magnetic field vectors ($\mathbf{E}$ and $\mathbf{H}$) can be considered as "vector voltages" and "vector currents", respectively. The field vectors in plane waves are orthogonal, therefore in order to make them aligned, $\mathbf{n} \times \mathbf{H}$ will be considered instead of $\mathbf{H}$. It is possible to express all the fields in terms of only tangential components. First, a metasurface between two media can be considered as a two-port network. Figure 2(a) presents a schematic of the problem. The performance of the metasurface can be described in terms of the so called

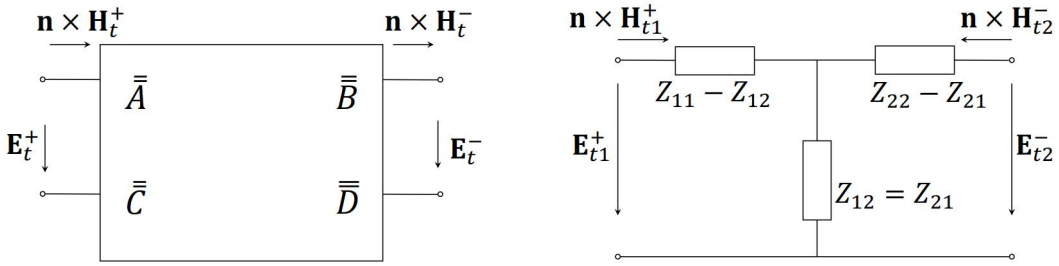

(a) (b)

Figure 2: (a) Representation of a metasurface as a two-port network. (b) Equivalent circuit for a metasurface in case of one polarization only.

$ABCD$-matrix,

$$\begin{pmatrix} \mathbf{E}_{\mathrm{t}}^+ \\ \mathbf{n}\times\mathbf{H}_{\mathrm{t}}^+ \end{pmatrix} = \begin{pmatrix} \bar{\bar{A}} & \bar{\bar{B}} \\ \bar{\bar{C}} & \bar{\bar{D}} \end{pmatrix} \cdot \begin{pmatrix} \mathbf{E}_{\mathrm{t}}^- \\ \mathbf{n}\times\mathbf{H}_{\mathrm{t}}^- \end{pmatrix}. \tag{16}$$

All the coefficients in the $ABCD$-matrix in the general case are dyadic. However, for the practical use, impedance matrix is more suitable than $ABCD$-matrix. Therefore, the same problem is rewritten in terms of the impedance matrix,

$$\begin{pmatrix} \mathbf{E}_{\mathrm{t}}^+ \\ \mathbf{E}_{\mathrm{t}}^- \end{pmatrix} = \begin{pmatrix} \bar{\bar{Z}}_{11} & \bar{\bar{Z}}_{12} \\ \bar{\bar{Z}}_{21} & \bar{\bar{Z}}_{22} \end{pmatrix} \cdot \begin{pmatrix} \mathbf{n}\times\mathbf{H}_{\mathrm{t}}^+ \\ \mathbf{n}\times\mathbf{H}_{\mathrm{t}}^- \end{pmatrix}. \tag{17}$$

Although a system of equations in (17) describes a uniform layer, it can be used to describe nonuniform metasurfaces. For this purpose, Z-parameters in (17) can be made dependent on the x and y coordinates. It will be considered thoroughly further, but let us first clarify the notion of perfect refraction by a metasurface.

2.2.1 Gradient metasurface based on the generalized Snell's law

Refraction of plane waves incident on an interface between two media is explained by Snell's law, which relates the incidence and refraction angles (θ_{i} and θ_{t}) with the refractive indices of the two media. The basis of this law is the continuity of the phase of electromagnetic waves across a homogeneous interface between the two media.

Plane waves in different media have different wavelengths, therefore, at the interface the wave must bend in order to preserve the phase continuity [8]. However, this relation can be broken by adding an additional phase shift at the interface between the media. In this case transmission is called anomalous and it is not described by Snell's law.

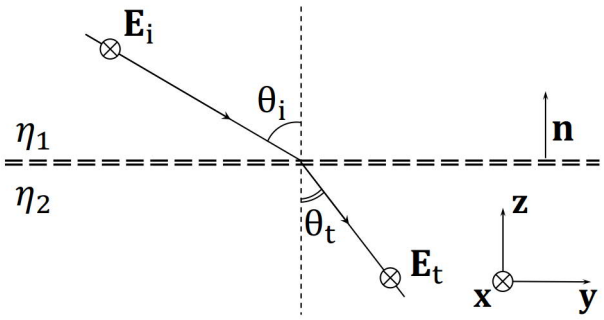

Figure 3: Schematic of an ideally refracting metasurface.

Metasurfaces add a certain phase shift to the incident field, therefore in order to describe reflection and refraction by a metasurface the Snell's law has to be modified. This was done in Ref. [9], where the generalized Snell's law was derived. Let us now consider this derivation, regarding metasurfaces for control of transmitted waves, which are called transmitarrays. In the following derivation the incident wave of only TE polarization will be considered. It is also assumed that the metasurface is located in the xy plane between the two media with characteristic impedances η_1 and η_2. Figure 3 represents schematic of the problem.

The tangential components of the incident and refracted electric fields can be written as:

$$\mathbf{E}_{t1} = E_{\mathrm{i}} e^{-jk_1 \sin\theta_{\mathrm{i}} y}\mathbf{x}, \qquad \mathbf{E}_{t2} = E_{\mathrm{t}} e^{-jk_2 \sin\theta_{\mathrm{t}} y + j\phi_t}\mathbf{x}, \tag{18}$$

where ϕ_t is an arbitrary phase shift and $\mathbf{x}$ is a unit vector along the x direction. Wave numbers in the first and second media are k_1 and k_2, respectively. The incident and refracted electric field amplitudes are denoted as E_{i} and E_{t}, they are assumed

to take real positive values. The angles of incidence and transmission are denoted as θ_i and θ_t, respectively. By using the equations in (18) the transmission coefficient can be derived:

$$T = \frac{\mathbf{x}\cdot\mathbf{E}_{t2}}{\mathbf{x}\cdot\mathbf{E}_{t1}} = \frac{E_\mathrm{t}e^{-jk_2\sin\theta_\mathrm{t}y+j\phi_\mathrm{t}}}{E_\mathrm{i}e^{-jk_1\sin\theta_\mathrm{i}y}} = Ae^{-jk_2\sin\theta_\mathrm{t}y+j\phi_\mathrm{t}+jk_1\sin\theta_\mathrm{i}y}, \tag{19}$$

where $A = E_\mathrm{t}/E_\mathrm{i}$. Equation (19) presents the transmission coefficient at each point of the metasurface. Although the wave numbers and angles are constants, the phase of the transmission coefficient depends on y linearly,

$$\Phi_\mathrm{t}(y) = \angle(E_{t2}/E_{t1}) = -k_2\sin\theta_\mathrm{t}y + \phi_\mathrm{t} + k_1\sin\theta_\mathrm{i}y. \tag{20}$$

By differentiating this equation along the y axis, the generalized Snell's law reads:

$$k_1\sin\theta_\mathrm{i} - k_2\sin\theta_\mathrm{t} = \frac{d\Phi_\mathrm{t}(y)}{dy}. \tag{21}$$

Equation (21) relates wave numbers in the media and the angles of incidence and transmission with the phase gradient along the y axis.

Although each point of the metasurface should provide a certain phase shift to the incident field, there is no need to vary the phase along the surface in infinite limits. It is possible to create a structure with a period D and vary the phase from 0 to 2π in the range of this period. Both of the angles and the wave numbers govern the period, which can be calculated as

$$\Phi_\mathrm{t}(z+D) = \Phi_\mathrm{t}(z) + 2\pi, \qquad D = \frac{2\pi}{|k_1\sin\theta_\mathrm{i} - k_2\sin\theta_\mathrm{t}|}. \tag{22}$$

By using only the generalized Snell's law it is possible to design a transmitarray. In general, the working principle of transmitarrays is illustrated in Fig. 4(a). For example, a normally incident plane wave obtains the phase profile, governed by the generalized Snell's law, and therefore it is transmitted at a certain angle. Figure 4(b) is a graphical representation of the generalized Snell's law. The phase profile along the metasurface should follow the solid line in Fig. 4(b). It is possible to utilize the circuit theory and define the Z-parameters that correspond to such phase profile. This idea was proposed and utilized in Ref. [7], so let us consider it thoroughly.

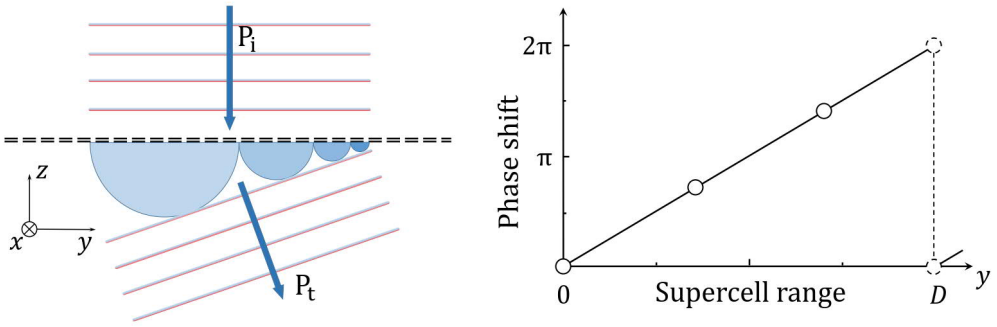

(a) (b)

Figure 4: Wavefront shaping by a transmitarray. (a) Representation of the metasurface as a set of secondary sources (Huygens' principle). (b) The phase profile along the metasurface. For the case of three inclusions per period D circles mark the phases shift cast by them.

Considering a metasurface as a homogeneous array and assuming $\eta_1 = \eta_2 = \eta_0$ enables to take $A = 1$ in Eq. (19). Under these assumptions it is possible to find the impedance matrices for the transmitarray. Considering the metasurface in terms of the circuit theory allows to express the impedance matrix by using the scattering parameters. By using standard equations for two-port networks, Z matrix elements can be expressed as

$$\begin{aligned}
Z_{11} &= \eta_0 \frac{(1+S_{11})(1-S_{22}) + S_{12}S_{21}}{(1-S_{11})(1-S_{22}) - S_{12}S_{21}}, \\
Z_{12} &= \eta_0 \frac{2S_{12}}{(1-S_{11})(1-S_{22}) - S_{12}S_{21}}, \\
Z_{21} &= \eta_0 \frac{2S_{21}}{(1-S_{11})(1-S_{22}) - S_{12}S_{21}}, \\
Z_{22} &= \eta_0 \frac{(1-S_{11})(1+S_{22}) + S_{12}S_{21}}{(1-S_{11})(1-S_{22}) - S_{12}S_{21}},
\end{aligned} \tag{23}$$

where η_0 is the characteristic impedance of the background medium, which is free space. In the design based on the generalized refraction law Z-parameters are chosen so that locally periodical arrays give the desired phase shifts and no reflections for all used values of Z-impedances. In this case the transmission coefficient is simply equal to scattering parameters S_{12} and S_{21}. Thereby, the phase variation along the

surface Φ_t governs the transmission coefficient, $T = e^{j\Phi_\mathrm{t}}$. As a result, equations in (23) can be rewritten as

$$Z_{11} = Z_{22} = j\frac{\eta_0}{\cos\theta_\mathrm{i}}\frac{1+T^2}{1-T^2} = j\frac{\eta_0}{\cos\theta_\mathrm{i}}\cot\Big(\Phi_\mathrm{t}(y)\Big),$$
$$Z_{12} = Z_{21} = j\frac{\eta_0}{\cos\theta_\mathrm{i}}\frac{1}{\sin\Big(\Phi_\mathrm{t}(y)\Big)}. \tag{24}$$

Impedances in (24) are purely imaginary, thus they define a lossless transmitarray. Nevertheless, metasurfaes that are designed by following this approach are not 100% efficient [10]. It can be shown by deriving a formula for the transmission efficiency. In order to do it, the impedances of the incident and transmitted waves should be introduced:

$$Z_\mathrm{in} = \frac{\eta_0}{\cos\theta_\mathrm{i}}, \quad Z_\mathrm{out} = \frac{\eta_0}{\cos\theta_\mathrm{t}}. \tag{25}$$

Since the energy cannot be absorbed, the reflection coefficient can be expressed as

$$R = \frac{Z_\mathrm{out} - Z_\mathrm{in}}{Z_\mathrm{out} + Z_\mathrm{in}} = \frac{\eta_0\cos\theta_\mathrm{i} - \eta_0\cos\theta_\mathrm{t}}{\eta_0\cos\theta_\mathrm{i} + \eta_0\cos\theta_\mathrm{t}}. \tag{26}$$

The reflection coefficient is not zero, because input and output impedances are not matched. The transmission coefficient amplitude can be expressed as

$$T = 1 + R = \frac{2\cos\theta_\mathrm{i}}{\cos\theta_\mathrm{i} + \cos\theta_\mathrm{t}}. \tag{27}$$

Power of the incident and transmitted waves can be found, by using the transmission coefficient amplitude:

$$P_\mathrm{in} = 1\cdot A^2\frac{\cos\theta_\mathrm{i}}{\eta_0}, \quad P_\mathrm{out} = T^2\cdot A^2\frac{\cos\theta_\mathrm{t}}{\eta_0}. \tag{28}$$

The transmission efficiency reads:

$$\xi = \frac{|P_\mathrm{out}|}{|P_\mathrm{in}|} = T^2\frac{\cos\theta_\mathrm{t}}{\cos\theta_\mathrm{i}}. \tag{29}$$

Figure 5 represents the efficiency estimation given by Eq. (29). In order to get this graph, the angle of incidence was fixed at $\theta_\mathrm{i} = 0°$ and the characteristic impedances of the media above and below the metasurface were assumed equal ($\eta_1 = \eta_2 = \eta_0$).

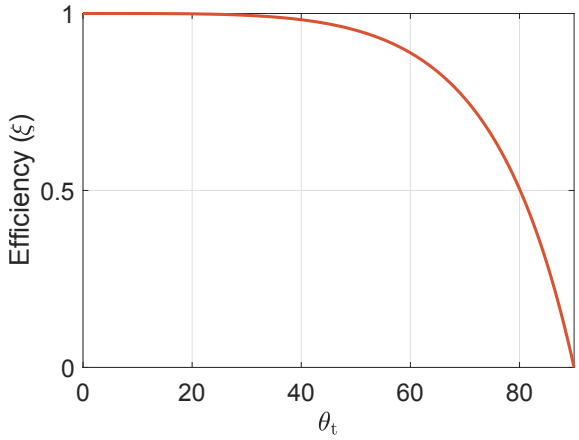

Figure 5: Efficiency of the transmitarray designed by following the generalized Snell's law as a function of the transmission angle. The graph was obtained under the assumptions: $\eta_1 = \eta_2 = \eta_0$ and $\theta_i = 0$.

2.2.2 Anomalous refractor without parasitic diffraction

Providing a proper phase match at each point, by following the generalized Snell's law, is a necessary condition, but not sufficient. The conditions for achieving ideal transmission were derived in Ref. [7], so let us now consider them. Coefficient A in Eq. (19) is not necessarily equal to 1, it can be either larger or smaller than 1. This becomes obvious simply comparing the widths of the incident and transmitted beams in Fig. 6.

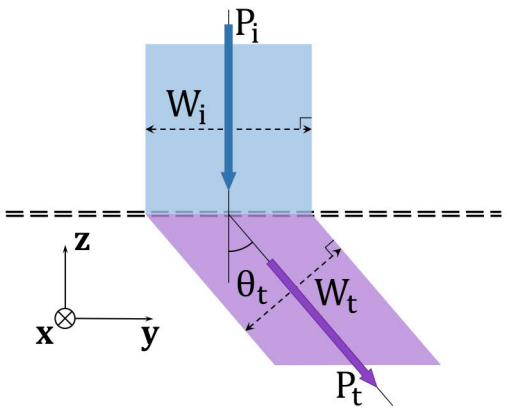

Figure 6: Schematic representation of power conservation in the ideal transmitarray.

Indeed, the beam becomes narrower after refraction, so in order to fulfill the power conservation rule, the amplitudes should be different. In other words, the amplitude of the transmitted light should be controlled in addition to the phase. It is possible to express one amplitude through another. In order to obtain such relation, we introduce tangential components of the incident and transmitted magnetic fields:

$$\mathbf{n}\times\mathbf{H}_{t1}=E_{\mathrm{i}}\frac{1}{\eta_1}\cos\theta_{\mathrm{i}}e^{-jk_1\sin\theta_{\mathrm{i}}y}\mathbf{x},\qquad \mathbf{n}\times\mathbf{H}_{t2}=E_{\mathrm{t}}\frac{1}{\eta_2}\cos\theta_{\mathrm{t}}e^{-jk_2\sin\theta_{\mathrm{t}}y+j\phi_{\mathrm{t}}}\mathbf{x}, \quad (30)$$

where $\mathbf{n}$ is the unit vector normal to the metasurface plane. The normal component of the Poynting vector at each point of the metasurface in both media can be expressed as:

$$\frac{1}{2}\mathrm{Re}(\mathbf{E}_{t1}\times\mathbf{H}^*_{t1})=\frac{1}{2}\mathrm{Re}(\mathbf{E}_{t2}\times\mathbf{H}^*_{t2}). \quad (31)$$

It is possible to write the transmitted field amplitude through the incident one by using equations (18), (30) and (31):

$$E_{\mathrm{t}}=E_{\mathrm{i}}\sqrt{\frac{\cos\theta_{\mathrm{i}}}{\cos\theta_{\mathrm{t}}}}\sqrt{\frac{\eta_2}{\eta_1}}. \quad (32)$$

It becomes clear now that the amplitude of the incident field can be larger or smaller than the amplitude of the transmitted field. Basically, Eq. (32) represents the boundary condition for lossless metasurfaces, when all the power is transmitted.

By using the field definitions in (18) and (30) and plugging them in (32) the Z-parameters for an ideal transmitarray can be determined. In order to do it, let us first rewrite matrix equation in (17) as a system of equations

$$\begin{aligned}\mathbf{E}_{t1}&=Z_{11}\mathbf{n}\times\mathbf{H}_{t1}+Z_{12}(-\mathbf{n}\times\mathbf{H}_{t2}),\\ \mathbf{E}_{t2}&=Z_{21}\mathbf{n}\times\mathbf{H}_{t1}+Z_{22}(-\mathbf{n}\times\mathbf{H}_{t2}),\end{aligned} \quad (33)$$

where all the dyadic Z-parameters were replaced with scalars. It is possible because all the dyadic coefficients share a common set of eigenvectors that correspond to different polarizations of incident field (TE and TM), thus in the basis of these vectors they become diagonal. Considering one polarization only allows to treat Z-parameters as scalars. Although in the following the incident wave of TE polarization will be considered, in a similar way it can be done for the TM polarization. The system of

equations in (33) can be considered by using an equivalent circuit, where $\mathbf{E}_{t1}$ and $\mathbf{E}_{t2}$ represent input and output voltages, respectively, and $\mathbf{n} \times \mathbf{H}_{t1}$ and $\mathbf{n} \times \mathbf{H}_{t2}$ stand for input and output currents. The equivalent circuit for reciprocal metasurfaces is depicted in Fig. 2(b).

Equations in (33) are written for one point on the metasurface only, thus in order to control transmission they should be solved for each point in the range of the period D, making the Z-parameters dependent on x and y. Using equations in (18), (30), (32) and (33) allows us to obtain the values of impedances for an ideal performance of the metasurface:

$$\begin{aligned} Z_{11} &= j\frac{\eta_1}{\cos\theta_\mathrm{i}}\cot\Phi_\mathrm{t}, \\ Z_{22} &= j\frac{\eta_2}{\cos\theta_\mathrm{t}}\cot\Phi_\mathrm{t}, \\ Z_{12} = Z_{21} &= j\frac{\sqrt{\eta_1\eta_2}}{\sqrt{\cos\theta_\mathrm{i}\cos\theta_\mathrm{t}}}\frac{1}{\sin\Phi_\mathrm{t}}. \end{aligned} \tag{34}$$

The metasurface designed by following equations in (34) is lossless and reciprocal. Indeed, all the Z parameters are purely imaginary and $Z_{12} = Z_{21}$. However, $Z_{11} \neq Z_{22}$, meaning that the metasurface is asymmetric. Such structure of the Z parameters corresponds to omega coupling. In other words, a transmitarray can be ideal if only it possesses bianisotropic response [7]. In practice, several topologies exist, that ensure bianisotropy of the metasurfaces, such as arrays of split rings and double arrays of patches [11, 12].

3 Realization of transmitarray metasurfaces

In the previous sections transmitarrays were considered from the theoretical point of view only. The conditions of an ideal performance were derived and on this basis it was shown that an ideal transmitarray should be bianisotropic. However, practical realization of the transmitarrays was not considered, therefore in this section possible ways for metasurface designs will be studied.

Previously in this work the metasurfaces were considered in terms of the impedance matrices, however it is more practical way to consider them by using scattering parameters. Basically, the Z parameters describe properties of the metasurface. Whereas the scattering parameters describe the response of the metasurface, which is measured. Both Z-parameters and S-parameters a equivalent, but scattering parameters are more suitable in this section. Equations in (23) relate the Z parameters with the scattering parameters, therefore the reverse equations can be easily derived.

In order to design a transmitarray, first, the wavefront has to be shaped. Namely the gradient metasurface provides a periodic response whose period D is defined by Eq. (22). This period can be considered as a supercell formed by a set of inclusions. Although the electromagnetic properties are varied along the whole metasurface, the properties in the range of one period govern the phase profile of the transmitarray. Therefore, designing one cell of the metasurface, which is called a supercell, the whole metasurface can be built.

The inclusions in the supercell can be designed by following two approaches. The first one is Eq. (23). It utilizes only the generalized Snell's law, therefore it will be called non-bianisotropic. By following this approach, the inclusions are designed locally to transmit incident light ideally ($|E_\mathrm{i}| = |E_\mathrm{t}|$), but with a certain phase ($\angle E_\mathrm{i} \neq \angle E_\mathrm{t}$). Schematically it is shown in Figure 7. Arranging all the inclusions in a supercell, the wavefront can be shaped. However, it was shown in the previous section, that efficiency of such designs cannot be 100% at large angles (see Fig. 5).

The second approach is Eq. (34). This approach assumes full control of not only the transmission phase but the amplitude also. In the previous part it was shown

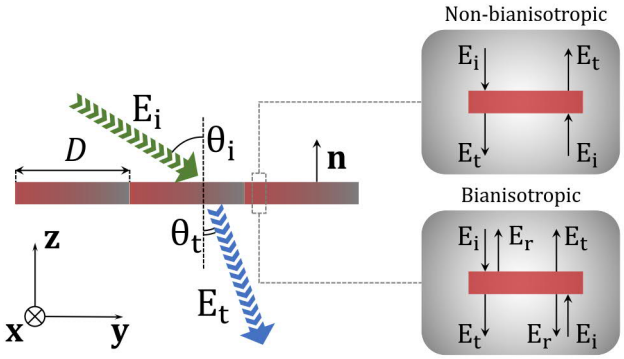

Figure 7: Schematic of a gradient metasurface. Insets represent different approaches to design inclusion of supercells.

that the inclusions for such metasurfaces should be bianisotropic. In order to follow this approach the inclusions should be designed so that the field locally should not be transmitted ideally ($|E_\mathrm{i}| \neq |E_\mathrm{t}|$). Therefore, each inclusion should reflect some light (E_r). However, a supercell composed of such inclusions transmits the light ideally. The exact values of the local reflection and transmission coefficients can be calculated by using the known Z parameters,

$$\begin{aligned}
S_{11} &= \frac{(Z_{11}-\eta_0)(Z_{22}+\eta_0)-Z_{12}Z_{21}}{(Z_{11}+\eta_0)(Z_{22}+\eta_0)-Z_{12}Z_{21}},\\
S_{12} &= \frac{2Z_{12}\eta_0}{(Z_{11}+\eta_0)(Z_{22}+\eta_0)-Z_{12}Z_{21}},\\
S_{21} &= \frac{2Z_{21}\eta_0}{(Z_{11}+\eta_0)(Z_{22}+\eta_0)-Z_{12}Z_{21}},\\
S_{21} &= \frac{(Z_{11}+\eta_0)(Z_{22}-\eta_0)-Z_{12}Z_{21}}{(Z_{11}+\eta_0)(Z_{22}+\eta_0)-Z_{12}Z_{21}}.
\end{aligned} \tag{35}$$

For the both approaches the transmission phase has to be controlled similarly. Previously, Fig. 4(b) showed that the phase should be gradually increasing from 0 to 2π in the range of one period. It means that the inclusions should be able to control the transmission phase in the same range. Because of the unlike properties of materials at different wavelengths, it is reasonable to consider the realization of metasurfaces in microwaves and optics separately.

3.1 Metasurfaces in microwaves

It was mentioned previously that the Z-parameters for nonuniform metasurfaces are dependent on the tangential coordinates (x and y). Although the Z-parameters should vary continuously, the metasurface is discretized for practical realizations. It means that the supercell is divided into a set of inclusions which mimic a smooth change of the Z-parameters. On the other hand, the impedance matrix contains four elements. By considering reciprocal metasurfaces only, the number of independent parameters reduces. Therefore, each inclusion is characterized by three independent Z-parameters. In practical realizations a sheet impedance of a layer can be tuned. Therefore, placing three of these impedance sheets in parallel allows us to assign three complex parameters to such system. By presenting the inclusion in form of three layers, it is also characterized by three sheet impedances. This idea was proposed in Refs. [13, 14]. For this approach, the circuit in Fig. 8 shows actual representation of the T-circuit in Fig. 2(b). It consists of three sheet impedances (Z_1, Z_2, Z_3) separated

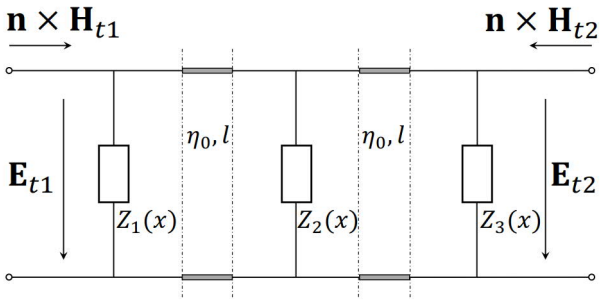

Figure 8: Actual representation of a metasurface for realizations with three impedance layers.

by transmission lines of length l and characteristic impedance of free space η_0. The required sheet impedances can be related with the Z-parameters in (24),

$$Z_1 = Z_3 = \frac{\eta_0(Z_{11}^2 - Z_{12}^2)\sin(k_0 l)}{j(Z_{11}^2 - Z_{12}^2)\cos(k_0 l) + \eta_0(Z_{11} + Z_{12})\sin(k_0 l)},$$
$$Z_2 = \frac{\eta_0^2 Z_{12}(\cos(2k_0 l) - 1)}{2(Z_{11}^2 - Z_{12}^2) - j\eta_0 Z_{12}\sin(2k_0 l)}, \tag{36}$$

where l is the distance between the layers and k_0 is wave number in free space.

Equations in (24) and (36) are equivalent. They describe an approach, which is based solely on the generalized Snell's law. Therefore, the metasurfaces, designed by following this approach, are symmetric ($Z_{11} = Z_{22}$), consequently, the impedance values assigned to the outer sheets are equal ($Z_1 = Z_3$).

In order to assure wavefront shaping, the period D was divided into 30 elements. Each inclusion is formed by three impedance sheets with different impedance values. Initially the metasurface was defined as an infinitely thin sheet, however in the

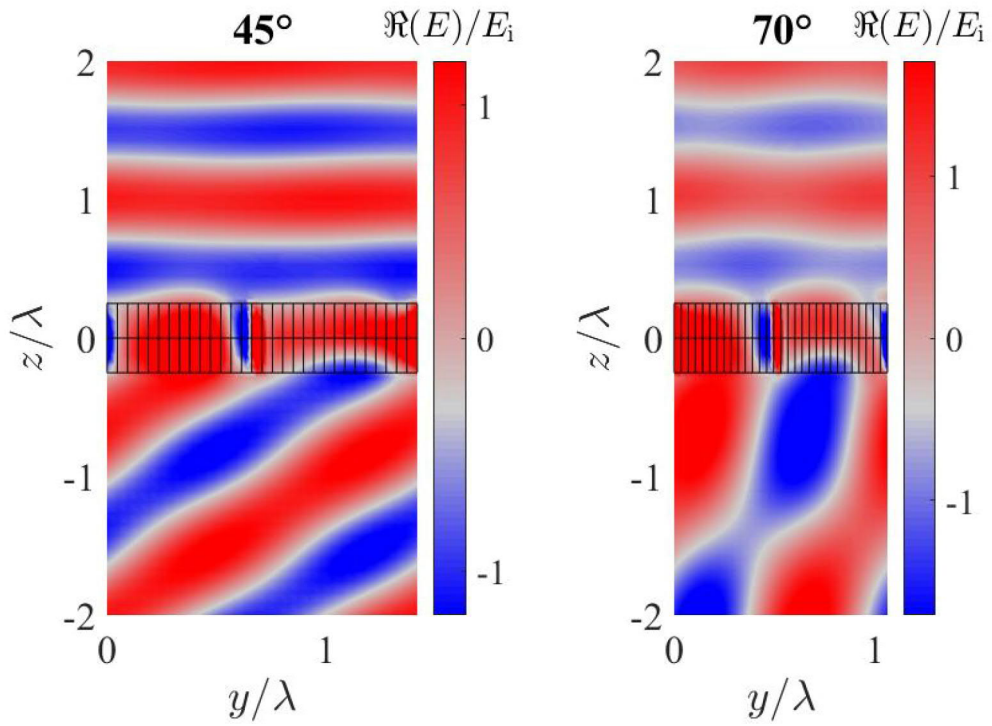

(a) (b)

Figure 9: Three layers simulations for wave control [14]. (a) The angle of transmission: 45°. (b) The angle of transmission: 70°.

simulations the distance between the layers is $\lambda/4$. Although the total thickness of the modeled metasurface is not zero, it is still less than the wavelength. The inclusions in the supercell have to be separated in order to prevent interaction between them. In order to decouple neighboring inclusions, they were separated by a perfect magnetic

conductor. Finally, by following the non-bianisotropic approach, two metasurfaces were simulated. They are designed to transmit normally incident light at angles of 45° and 70°. Figure 9 shows the electric field distributions for both of the metasurfaces.

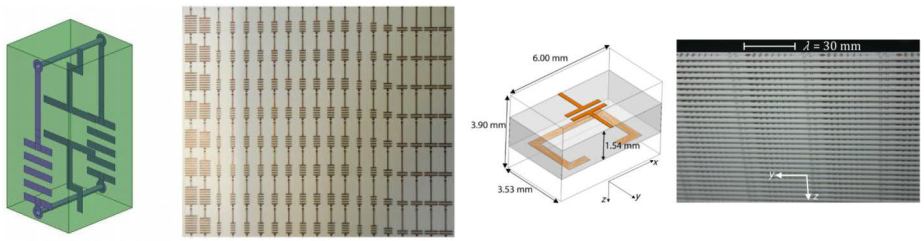

(a) (b)

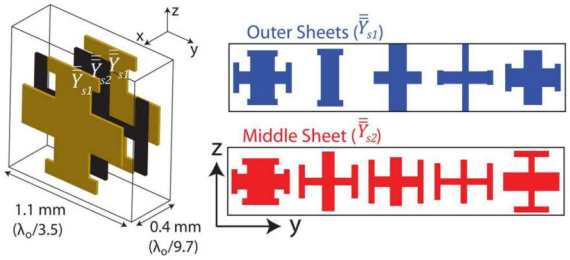

(c)

Figure 10: Non-bianisotropic structures forming gradient transmitarrays. (a) A scheme of non-bianisotropic cell and a photo of a transmitarray made of loaded loops and wires working at frequency $f = 10$ GHz [15]. (b) Scheme of a symmetric cell and a photo of a transmitarray working at $f = 10$ GHz [13]. (c) The size parameters of a unit cell and schemes of the layers of the supercell working at $f = 77$ GHz [16].

In the first case, when the angle of transmission is 45°, the reflections cause a minor effect on the performance. The efficiency of these designs depending on the transmission angle is presented in Fig. 5. For the angle of 45° the efficiency is close to 100%. However, for the angle of 70° imperfection of this approach is obvious. According to the efficiency curve in Fig. 5, approximately 76% of the incident power

is transmitted at the angle of 70°. The obtained results represent a theoretical model, where all the parameters do not depend on the wavelength. Therefore, all of the equations are valid at any frequency. However, this theory is more applicable in the micro and radio frequency ranges [13–19]. Examples of non-bianisotropic designs are presented in Fig. 10. Unit cells used in these designs are symmetric, therefore these structures are truly non-bianisotropic. All the inclusions were designed to give a certain phase shift to the incident field with no reflections. As a result, the efficiency of these designs does not exceed the theoretical limit for non-bianisotropic designs in Fig. 5.

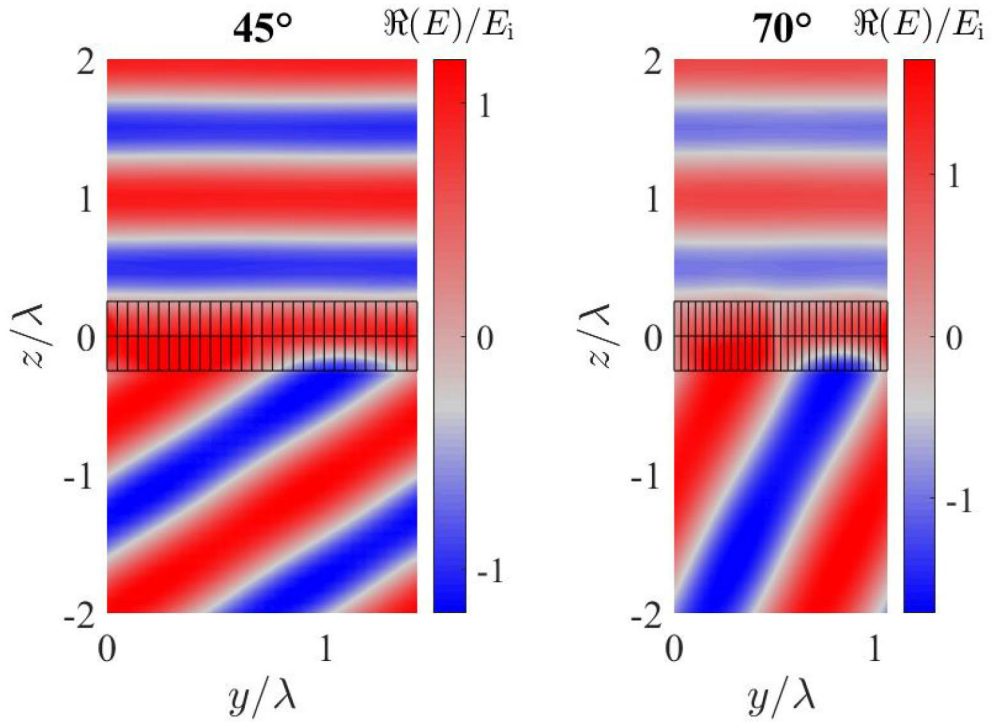

(a) (b)

Figure 11: Representation of the bianisotropic approach by simulations with three layers impedance model [14]. (a) the angle of transmission: 45°. (b) the angle of transmission: 70°.

Another approach is based on bianisotropic elements, it allows designing ideal transmitarrays. The metasurfaces of this type are reciprocal ($Z_{12} = Z_{21}$) and

asymmetric ($Z_{11} \neq Z_{22}$). Therefore three values of Z-parameters in (34) has different values. It means that for three layer simulation impedance values assigned to the sheets are all different. Expressing the Z-parameters for three layer simulations (Z_1, Z_2, Z_3), by using the Z-parameters from the equations in (34), gives

$$Z_1 = \frac{\eta_0(Z_{11}Z_{22} - Z_{12}^2)\sin(k_0 l)}{j(Z_{11}Z_{22} - Z_{12}^2)\cos(k_0 l) + \eta_0(Z_{22} + Z_{12})\sin(k_0 l)},$$
$$Z_2 = \frac{\eta_0^2 Z_{12}(\cos(2k_0 l) - 1)}{2(Z_{11}Z_{22} - Z_{12}^2) - j\eta_0 Z_{12}\sin(2k_0 l)},$$
$$Z_3 = \frac{\eta_0(Z_{11}Z_{22} - Z_{12}^2)\sin(k_0 l)}{j(Z_{11}Z_{22} - Z_{12}^2)\cos(k_0 l) + \eta_0(Z_{11} + Z_{12})\sin(k_0 l)}. \quad (37)$$

By using these values of impedances, two metasurfaces were modeled to transmit waves at the same as previously angles, 45° and 70°. Figure 11 represent the electric field distribution for these metasurfaces. It is clear that both these transmitarrays produce no reflections, therefore both of them are ideal.

Metasurfaces in [17, 18, 20–22] can be considered as examples of bianisotropic metasurfaces. Three sheet impedance model was utilized in [18, 21, 22]. Figure 12 shows schematics of unit cells and supercells used in the works. Efficiency of the transmitarrays, designed in [18, 22], exceed the theoretical limit of non-bianisotropic designs (see Fig. 5). Therefore, these works prove that full controll of transmitted wave (amplitude and phase) is possible by using only bianisotropic metasurfaces.

3.2 Metasurfaces in optics

First gradient metasurface in optics was demonstrated in the same paper where the generalized Snell's law was introduced [9]. This work showed that linear phase gradient introduced by the metasurface can change the propagation direction of the incident light breaking the traditional Snell's law. This effect is also known as anomalous refraction or reflection. Figure 13(a) schematically shows the wavefront shaped by a supercell of antennas in [9]. The introduced metasurface is a frequency selective surface (FSS) where the control of the phase change along the metasurface is provided by metallic V-shaped antennas. Such structures introduce the electric response only, as most of the conventional designs do that are based on FSS. Non-

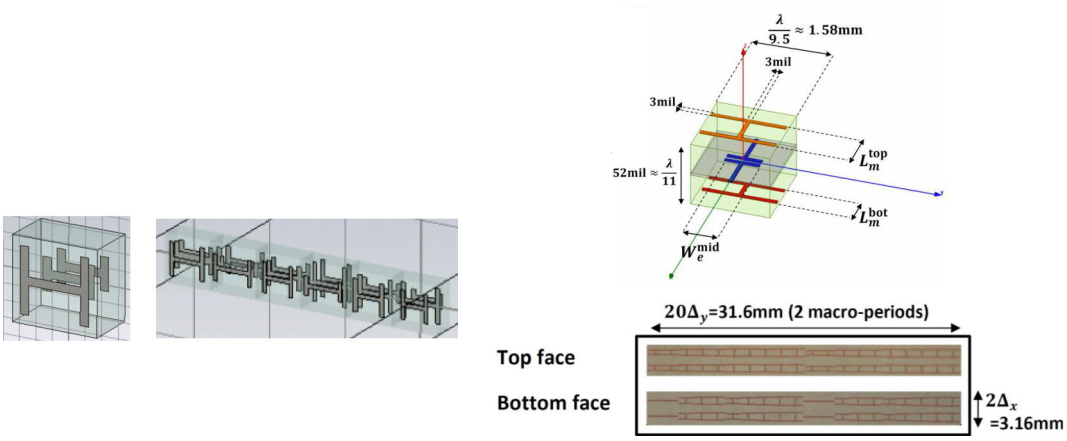

(a) (b)

Figure 12: Bianisotropic transmitarray designs. (a) Schematics of a unit cell and a super cell. This design works at $f = 10.5$ GHz [22]. (b) Schematic of a unit cell and a photo of transmitarray working at $f = 20$ GHz [18].

desired reflections, refractions and polarization conversions limit the efficiency of such designs by the value of 25%. Even though this design is non-bianisotropic and the efficiency has a theoretical limit below 100%, angles at which this design works are small, therefore this cause a minor effect on the efficiency.

Another example of a non-bianisotropic metasurface operating in the optical range is presented in [19]. Figure 13(b) shows the structure implemented in this work. Diagonal elements of the impedance matrix, Z_{11} and Z_{22}, are matched to be equal. In terms of the three-layer model, the substrate was considered as a part of one of the layers. For this reason, even though the inclusions in this design are asymmetric, they are still non-bianisotropic. This structure transmits 30% of incident light at the angle of 35°. Different metasurface that transmits light at the angle of 30° is presented in [23]. Figure 13(c) shows schematics of the unit cell and the supercell of the implemented structure. The efficiency of 75% was achieved in simulations. Worth noting that for both designs in [19] and [23] the limiting efficiency at the angles below 40° is almost 100%. However, both these designs are plasmonic and operate at the resonance. Due to the presence of free carrier in metals, such metasurfaces are lossy. In addition to that, magnetic response saturated due to the plasmonic properties of

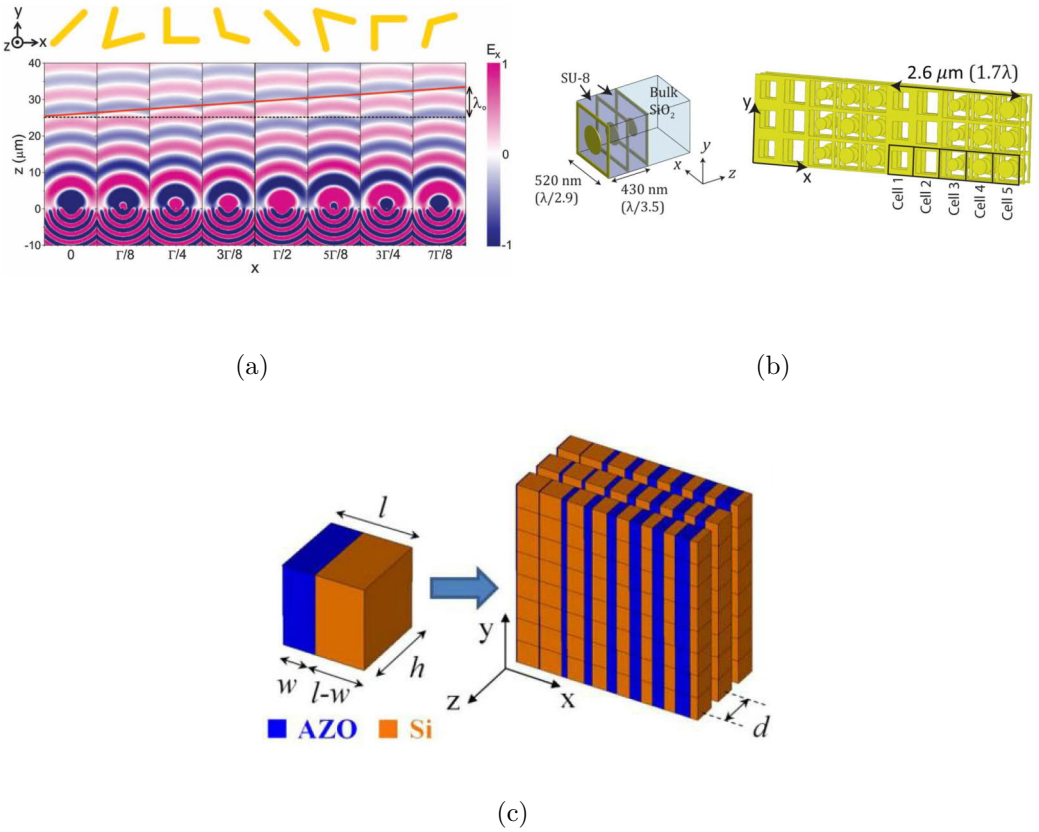

(a) (b)

(c)

Figure 13: Non-bianisotropic transmitarrays in optics. (a) A scheme of a metasurface that works at the wavelength of 8 μm. The wavefront shaping, by following the generalized Snell's law, is schematically presented [9]. (b) Schematic of a three layer unit cell forming a transmitarray at the wavelength of 1.5μm [19]. (c) Symmetric three-layer unit cell made of AZO-silicon plasmonic nanorods, forming a supercell. This design works at the wavelength of λ=3μm [23].

metals [24]. Therefore, in order to increase the efficiency of metasurfaces in optics, the inclusions should not be plasmonic.

All the limitations, connected with the use of metals, have to be overcome. In order to do it all-dielectric inclusions can be used instead of metallic ones. Dielectric nanoparticles can support both magnetic and electric dipolar modes and at the optical frequencies they possess very low intrinsic losses [25]. Changing the geometrical parameters of the particles allows tuning the magnetic and electric resonances.

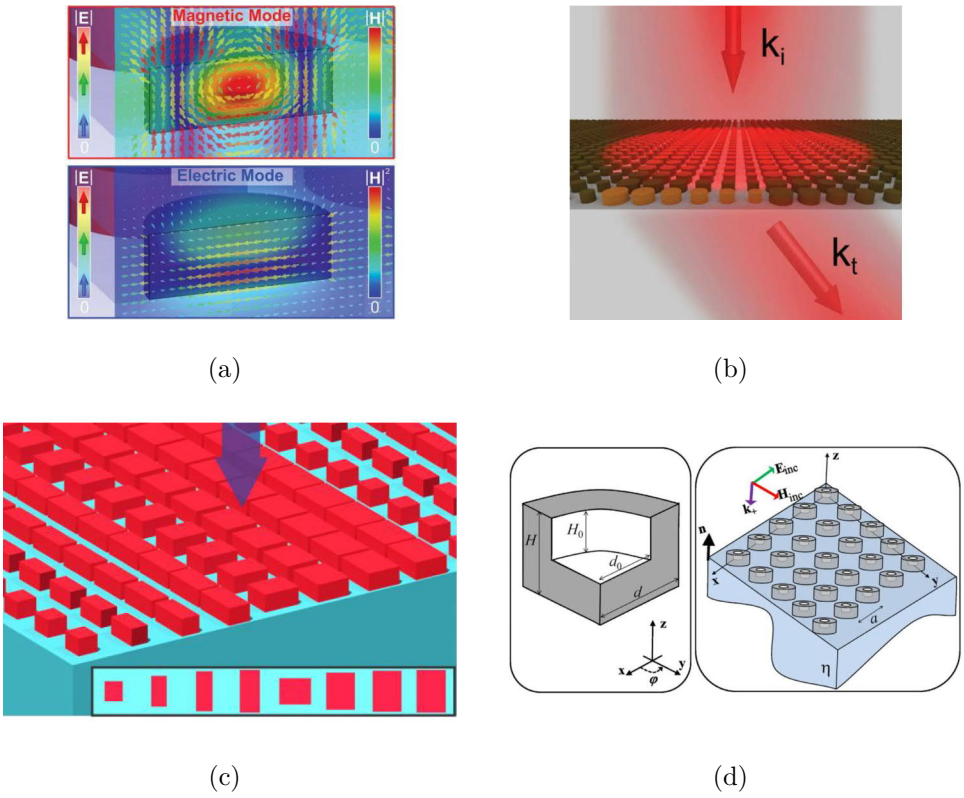

(a) (b)

(c) (d)

Figure 14: Realization of transmitarrays in optics. (a) Schematics of the electric and magnetic field distributions at the resonances [25]. (b) and (c) Transmitarrays made of silicon cylinders [26] and nanoblocks [27]. (d) Schematic of a bianisotropic metasurface made of dielectric inclusions [28].

Figure 14(a) represent schematics of the electric and magnetic field distributions at the resonant frequencies. Each of the resonances give π phase shift to the transmission field, therefore spectrally overlapping both resonances provides full 2π phase coverage [25]. This idea was implemented for simple structures such as cylinders [26] and blocks [27]. Figure 14(b,c) represent these metasurfaces. The efficiencies of these designs are 45% and 36%. Both these designs still are non-bianisotropic, because the inclusions are symmetric and the amplitude was not controlled.

All-dielectric bianisotropic inclusions were introduced in [28]. Figure 14 shows schematic of the structure implemented in that work, which is, basically, a set all-dielectric omega particles. Although a clear advantage of bianisotropic metasurfaces

was not shown in optics, it was in the microwave region [18, 22]. In general, the difference between bianisotropic and non-bianisotropic designs is insignificant at small angles. However, metasurfaces operating at large angles ($\theta_t > 60^\circ$) with high efficiency should be bianisotropic (see Fig. 5). In addition to that, in order to avoid the limitations of the efficiency connected with the use of metals, only all-dielectric materials should be used.

4 Full phase control by only dipole response

Previously, different theoretical approaches that enable characterization of metasurfaces were considered. It was shown, that in order to design a transmitarray according to Eq. (21), the phase change along the surface should be varied in the range from 0 to 2π. Therefore, by designing inclusions that can control the transmission amplitude and phase in the desired range, the transmitarray can be obtained. Although different realization approaches of metasurfaces in microwaves and optics were considered, designs of inclusions in optics was not discussed thoroughly. Therefore, in this section design of a unit cell in optics will be considered.

Let us begin with an electrically thin planar layer illuminated by an arbitrary plane wave with frequency ω. The electromagnetic response of this layer can be described, by using the generalized sheet transition conditions, (11) and (12). These equations relate the field jumps across the metasurface and the polarization density vectors. Although a metasurface is defined as a thin layer, it can be polarized normally. Therefore the polarization density vectors for a metasurface contain two normal components (P_{n} and M_{n}) in addition to two tangential ones ($\mathbf{P}_{\mathrm{t}}$ and $\mathbf{M}_{\mathrm{t}}$). However, the polarization and the angle of incidence of the excitation wave define the number of non-zero components of the polarization density vectors.

4.1 Normal incidence

Let us start the analysis by considering a metasurface which is normally illuminated by an incident plane wave. Normal components of the averaged polarization vectors ($\mathbf{P}_{\mathrm{n}}$ and $\mathbf{M}_{\mathrm{n}}$) are zero, because the structure is fully symmetric with respect to the metasurface plane, thus the conditions (11) and (12) can be modified:

$$\mathbf{E}_{\mathrm{t}}^{+} - \mathbf{E}_{\mathrm{t}}^{-} = j\omega\mathbf{n} \times \mathbf{M}_{\mathrm{t}}, \tag{38}$$

$$\mathbf{n} \times \mathbf{H}_{\mathrm{t}}^{+} - \mathbf{n} \times \mathbf{H}_{\mathrm{t}}^{-} = j\omega\mathbf{P}_{\mathrm{t}}, \tag{39}$$

These equations show that the field jumps cast by normally illuminated metasurface can be produced by the tangential components of the polarization vectors, $\mathbf{P}_{\mathrm{t}}$ and $\mathbf{M}_{\mathrm{t}}$.

Since they are the only components that can be excited, they are the only ones that can resonate.

Let us rewrite the boundary conditions in (38) and (39) by using electric and magnetic fields, defined in (18) and (30). Both the conditions can be expressed in terms of the incident ($\mathbf{E}_\mathrm{i}$), reflected ($\mathbf{E}_\mathrm{r}$) and transmitted ($\mathbf{E}_\mathrm{t}$) fields as

$$\begin{aligned} \mathbf{E}_\mathrm{i} + \mathbf{E}_\mathrm{r} - \mathbf{E}_\mathrm{t} &= j\omega \mathbf{n} \times \mathbf{M}_t, \\ \Big(E_\mathrm{i} - E_\mathrm{r} - E_\mathrm{t}\Big)\mathbf{y} &= j\omega\eta_0 \mathbf{P}_t \times \mathbf{n}. \end{aligned} \tag{40}$$

The polarization vectors can be expressed, by using the dipole moments, $\mathbf{P}_\mathrm{t} = \mathbf{p}/S$ and $\mathbf{M}_\mathrm{t} = \mathbf{m}/S$. Dipole moments, in turn, can be expressed in terms of the incident electric and magnetic fields, resulting in

$$\mathbf{P}_\mathrm{t} = \frac{\hat{\alpha}^\mathrm{ee}\mathbf{E}_\mathrm{i}}{S}, \quad \mathbf{M}_\mathrm{t} = \frac{\hat{\alpha}^\mathrm{mm}\mathbf{H}_\mathrm{i}}{S} \tag{41}$$

where S is the unit cell area. It was assumed that the layer is non-bianisotropic ($\hat{\alpha}^\mathrm{em} = \hat{\alpha}^\mathrm{me} = 0$). By using the definition in (30), Eqs. (38) and (39) can be expressed in terms of the electric fields only,

$$\begin{aligned} -(E_\mathrm{i} + E_\mathrm{r} - E_\mathrm{t})\mathbf{y} &= -j\omega\frac{\hat{\alpha}^\mathrm{mm}E_\mathrm{i}}{S\eta_0}\mathbf{y}, \\ \Big(E_\mathrm{i} - E_\mathrm{r} - E_\mathrm{t}\Big)\mathbf{x} &= j\omega\eta_0\frac{\hat{\alpha}^\mathrm{ee}E_\mathrm{i}}{S}\mathbf{x}. \end{aligned} \tag{42}$$

Obviously, we can consider only the lengths of the vectors. By dividing both these equations by E_i, it is possible to sum these equations. The resulting expression gives the formula for the reflection coefficient,

$$R = -\frac{j\omega}{2S}\eta_0\hat{\alpha}^\mathrm{ee} + \frac{j\omega}{2S}\frac{\hat{\alpha}^\mathrm{mm}}{\eta_0}. \tag{43}$$

Assuming that at the electric and magnetic resonances occur at different frequencies allows to consider the resonances separately. Let us first consider the electric resonance. In the absence of losses the polarizabilities at the resonance are defined as [29]

$$\hat{\alpha}^\mathrm{ee} = \frac{2S}{j\omega\eta_0}, \quad \hat{\alpha}^\mathrm{mm} = 0. \tag{44}$$

The reflection coefficient at the electric resonance can be calculated by using Eq. (43), $R = -1$. It means that at the electric resonance the incident light is fully reflected

with the phase $-\pi$. Considering further the magnetic resonance, the polarizabilities can be described as [29]

$$\hat{\alpha}^{\mathrm{ee}} = 0, \quad \hat{\alpha}^{\mathrm{mm}} = \frac{2S\eta_0}{j\omega}. \tag{45}$$

The reflection coefficient in this case is $R = 1$, therefore the incident light is fully reflected with the phase 0. At wavelengths, far from the resonant, both of the polarizabilities are almost zero, therefore the reflection coefficient is approaching 0. In other words, at non-resonant wavelengths the dipole moments are not excited, therefore the light is fully transmitted through the layer.

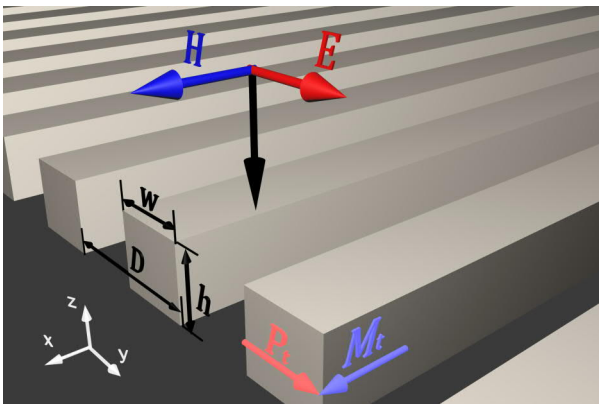

Figure 15: A periodic array of dielectric bars under normal illumination. The refractive index of the dielectric material is $n_{\mathrm{d}} = 6$ and the periodicity is $D = 730$ nm and the width of bars is $w = 300$ nm and the height is $h = 360$ nm.

Let us now check these equations in the simulations. Figure 15 represents the studied structure. It is a periodic array of dielectric bars illuminated normally by a plane wave of TM polarization (**E** is perpendicular to the strips). In order to ensure explicit demonstration of the results, the refractive index of the dielectric is $n_{\mathrm{d}} = 6$ and losses are neglected, at this point of the analysis.

The results of the simulations are presented in Fig. 16. The reflection spectrum in Fig. 16(a) shows two maxima, which correspond to the dipole resonances. At the resonance at the wavelength of 1.92 μm the phase of the reflected light is approximately $-\pi$. The second resonance is at the wavelength of 2.68 μm. The reflection phase is close to 0, therefore the first reflection maximum (1.92 μm) corresponds to the

electric dipole resonance, the second (2.68 μm) to the magnetic. The electric field distributions at these wavelengths are presented in Fig. 16(b) and (c). At the first resonance, the electric field inside the bars is directed along the incident field, demonstrating that the resonance corresponds to the electric dipole. The electric field at the second resonance is rotating inside the bars, producing the magnetic dipole, resonating along the bars.

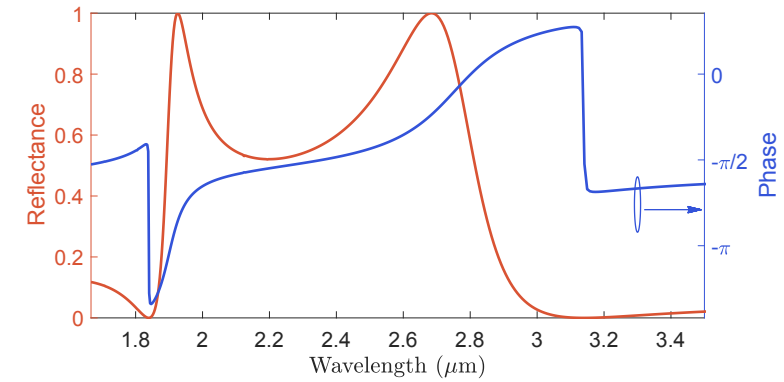

(a)

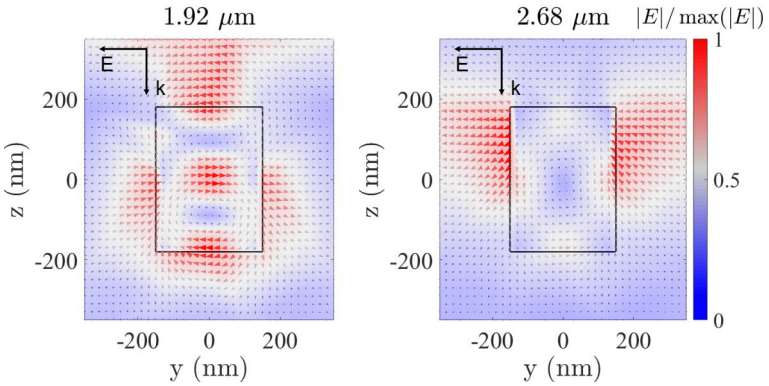

(b) (c)

Figure 16: (a) The magnitude and phase of the reflection coefficient. (c) and (d) The electric field distribution at wavelengths 1.92 μm and 2.68 μm, which correspond to electric and magnetic dipole resonances, respectively.

Each resonance gives a π phase shift to the transmitted field, thus spectrally overlapping these resonances full phase control can be obtained. It means that both resonances should be excited at one wavelength. Therefore, both of the polarizabil-

ities ($\hat{\alpha}^{\mathrm{ee}}$ and $\hat{\alpha}^{\mathrm{mm}}$) in Eq. (43) are not zero. In other words, the fields, radiated by the induced dipole moments should cancel each other in reflected direction. As a result, the incident light is fully transmitted with the phase change of 2π at the resonant wavelength.

This principle was introduced in [25], and utilized for simple geometries such as cylinders [26] and nanoblocks [27]. Obtaining electric and magnetic resonances at a single frequency was considered as an essential part of these designs. However, for some structures the resonances might occur at frequencies far from each other and bringing them together might be problematic. Besides of that, the origin of these resonances is different, therefore their properties change differently with the frequency. It means that full phase control is provided in a very narrow range of wavelengths. Both these factors can be overcome by changing the angle of the incidence from normal to an oblique one. This provides additional responses that allow us to obtain 2π phase shift by using only the electric or only the magnetic responses.

4.2 Oblique incidence

Considering a layer illuminated normally by a plane wave, derivation is identical for both polarizations. However, at an oblique incidence the symmetry breaks and the normal component of the polarization density vectors (M_{n} and P_{n}) are not zero. By choosing the incident light of TM polarization, the normal component of the magnetic polarization density vector, M_{n}, is zero. As a result, the generalized sheet boundary conditions in (11) and (12) can be specified as

$$\begin{aligned} \mathbf{E}_{\mathrm{t}}^{+} - \mathbf{E}_{\mathrm{t}}^{-} &= j\omega \mathbf{n} \times \mathbf{M}_{\mathrm{t}} - \nabla_t \frac{P_{\mathrm{n}}}{\varepsilon}, \\ \mathbf{n} \times \mathbf{H}_{\mathrm{t}}^{+} - \mathbf{n} \times \mathbf{H}_{\mathrm{t}}^{-} &= j\omega \mathbf{P}_{\mathrm{t}}. \end{aligned} \tag{46}$$

In comparison to the normal incidence, equations in (46) contain an additional term, which is the normal component of the electric polarization density, P_n. Since this response can be excited, it can resonate. Equations in (46) show that field jumps cast by a metasurface at oblique incidence can be produced by not only tangential but also normal components of the polarization density vectors.

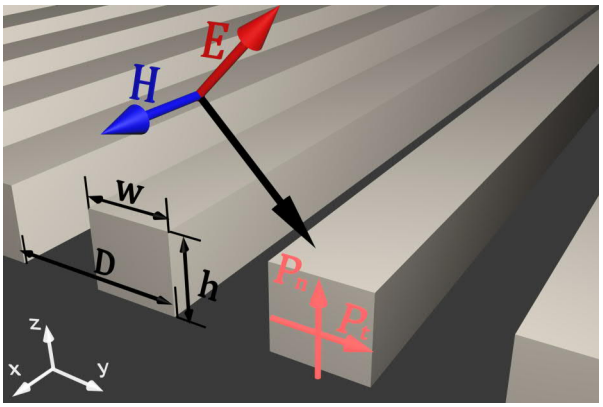

Figure 17: Schematic representation of a periodic array of bars. The refractive index of the dielectric material is $n_{\mathrm{d}} = 6$, the periodicity is $D = 730$ nm, the width of bars is $w = 300$ nm, the height is $h = 360$ nm.

Let us now consider a real metasurface at an oblique incidence. As it was for the normal incidence, the same periodic array of infinitely long bars will be considered. For simplicity, the illumination of this structure by a plane wave of TM polarization (**H** is along the bars) will be considered. The angle of incidence is 45°. Figure 17 shows the system under the study. As it was discussed previously, in order to ensure an explicit demonstration of the phenomenon, the refractive index of the dielectric is $n = 6$ and losses are neglected. The period of the array is $D = 730$ nm, the width is $w = 300$ nm, and the height is $h = 360$ nm.

The reflection spectrum and phase are plotted in Fig. 18(a). The reflection spectrum has three maxima. They correspond to the resonances excited in the metasurface. In comparison to the normal incidence, at oblique incidence three resonances are excited. The reflection phases at the wavelengths of 1.91 μm is approximately $-\pi$. Consequently, the reflection maximum at the wavelength of 1.91 μm corresponds to the resonating tangential component of the electric polarization density vector ($\mathbf{P}_t$). The reflection phase at the wavelengths of 2.70 μm is approximately 0 meaning that the reflection maximum at this wavelength corresponds to the resonating tangential component of the magnetic polarization density vector ($\mathbf{M}_t$). At the wavelength of 1.69 μm the incident light is fully reflected with the phase -2π. This resonance corresponds to the resonating normal component of the electric polarization den-

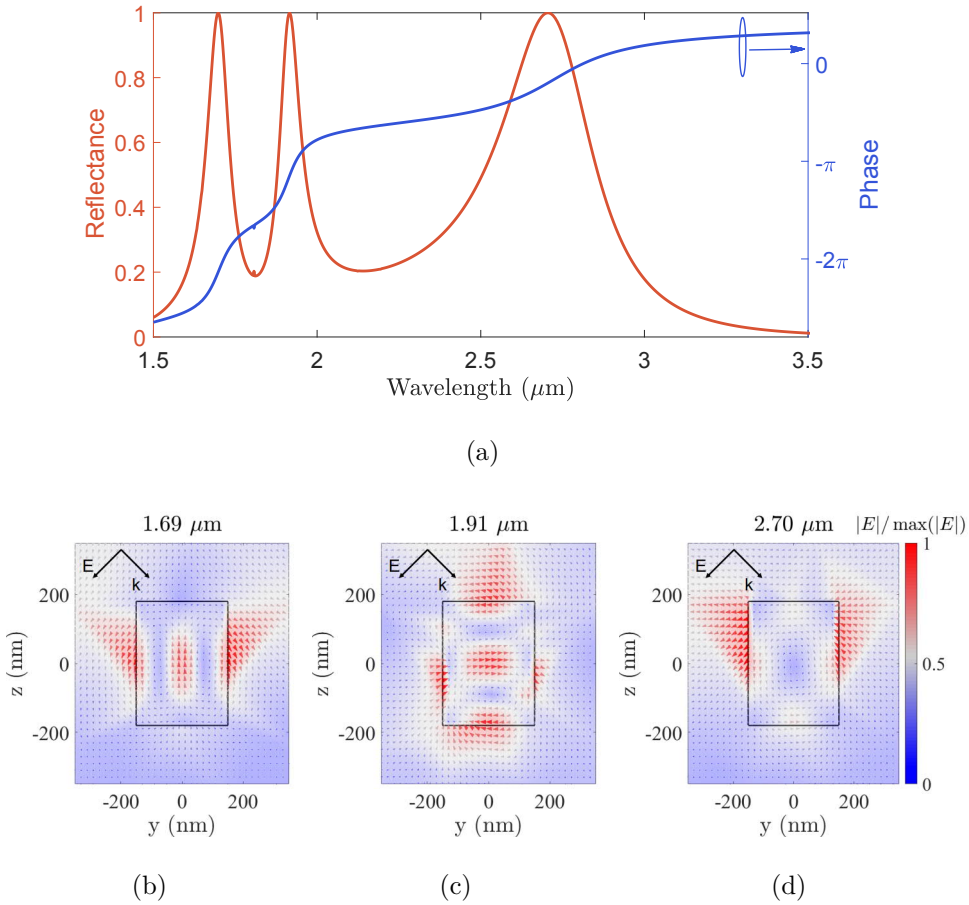

(a) (b) (c) (d)

Figure 18: (a) The magnitude and phase of the transmission coefficient. (b), (c) and (d) The electric field distribution at wavelengths 1.69 μm, 1.91 μm and 2.70 μm, respectively.

sity vector P_n. The electric field distributions in these points are presented in Fig. 18(b,c,d). The electric dipole moments, excited normally to the metasurface and in the metasurface plane, are demonstrated at the wavelength of 1.69 μm and 1.91 μm, respectively. On the other hand, the electric field at the wavelengths of 2.70 μm in Fig. 18(d) is circulating. It means that at this wavelength the magnetic dipole is resonating. Each of the resonances gives a π phase shift to the transmission field, thus, any of them can be used in order to obtain the phase coverage of 2π. Unlike previous works [25–28], in this work the electric response of the metasurface will be used, in order to obtain full 2π phase control.

By varying the shape parameters of the bars, electrical responses can be tuned to

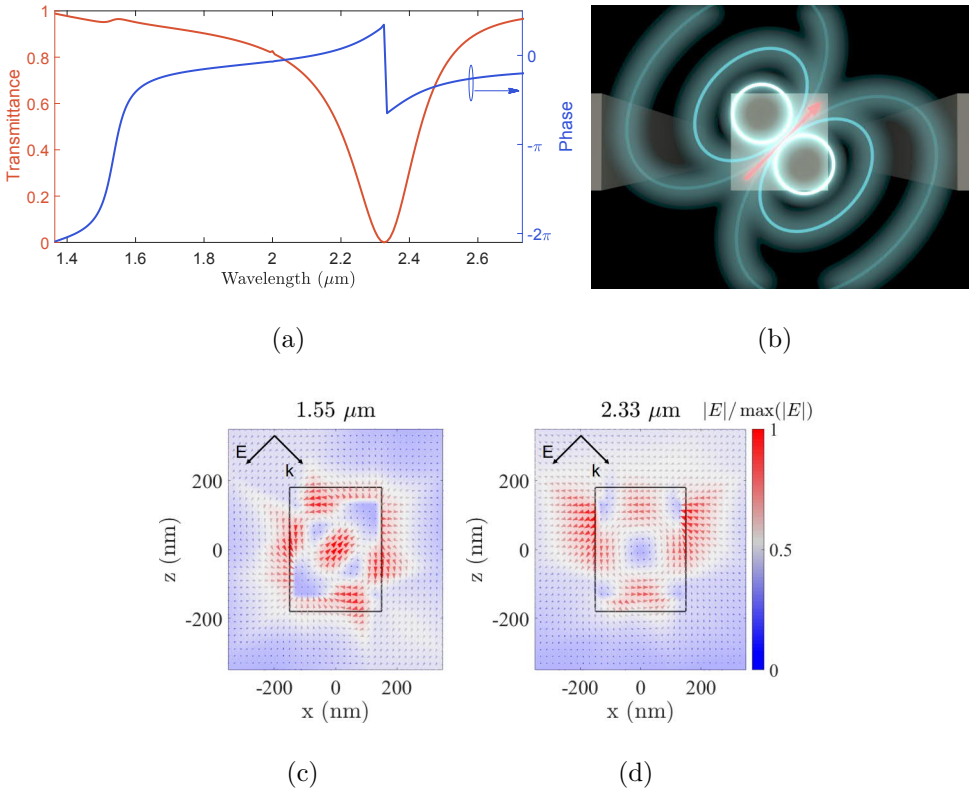

Figure 19: A periodic array of dielectric strips under oblique illumination. The refractive index of the dielectric material is $n_{\mathrm{d}} = 6$, the periodicity is $D = 730$ nm, the width of bars is $w = 280$ nm, and the height is $h = 275$ nm. (a) The magnitude and phase of the transmission coefficient for overlapped electric resonances. (b) Schematic representation of the total electric dipole moment. (c) and (d) The electric field distribution at wavelengths of 1.55 μm and 2.33 μm, which corresponds to tilted electric electric resonance and magnetic dipole resonance, respectively.

match at a certain wavelength. Figure 19(a) shows the transmission spectrum for an array of bars. The period of the array is $D = 730$ nm, the width is $w = 280$ nm and the height is $h = 275$ nm. At the wavelength of 1.55 μm both electric polarization density vectors ($\mathbf{P}_{\mathrm{t}}$ and $\mathbf{P}_{\mathrm{n}}$) are resonating. The total electric polarization vector is a superposition of the two induced dipole moments. Figure 19(b) schematically shows the induced dipole moment at the wavelength of 1.55 μm which provides the phase coverage of 2π. The electric field distribution at this wavelength is presented in Fig. 19(d). Only electric dipoles are excited at the wavelength of 1.55 μm,

whereas the magnetic dipole is excited at the wavelength of 2.33 μm. The electric field distribution at this wavelength in Fig. 19(c) is circulating, meaning that this resonance is a magnetic one. As a result, near the wavelength of 1.55 μm full phase coverage is obtained by using only the electric responses of the bars.

4.3 Eigenmode analysis

The previous analysis considered a metasurface by using the generalized sheet transition conditions. However, a real structure is formed by a set of inclusions. Each of these inclusions represents a resonator which supports eigenmodes of certain wavelengths. When an eigenmode is excited, the incident wave is fully reflected. The wavelengths of the eigenmodes are defined by the shape parameters of the resonators. However, a metasurface is represented by an array of resonators, therefore instead of a single resonator all of them should be analyzed together. An array of resonators is also a resonating system with its eigenmodes. Therefore, the metasurface can be described by analyzing its eigenmodes.

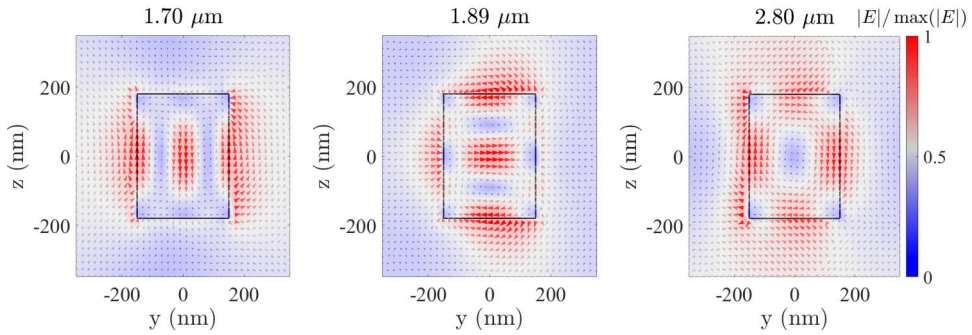

Figure 20: Eigenmode analysis of the array of bars made of dielectric material with the refractive index $n_{\mathrm{d}} = 6$. The periodicity of the structure is $D = 730$ nm, the width of bars is $w = 300$ nm and the height is $h = 360$ nm. (a), (b) and (c) The electric field distributions of the excited modes.

In general, properties of a system of resonators are described not only by their shape parameters but also by coupling between them, which can be controlled by the

distance between the resonators. By choosing the dimensions of the structure as in the previous analysis when resonances were not tuned ($D = 730$ nm, $w = 300$ nm, and $h = 360$ nm), the results can be compared. Modeling a unit cell and setting periodic boundary conditions enables us to simulate an array of resonators. The excitation angle can be controlled by changing the phase along the boundaries. In order to simulate the same structure as in the previous analysis, the angle of incidence was set to 45°. The propagating eigenmodes of the structure were excited at the wavelengths of 1.70 μm, 1.89 μm and 2.80 μm. Based on the electric field distributions in Fig. 20 the origins of the eigenmodes can be specified. The eigenmodes excited at the wavelengths of 1.70 μm and 1.89 μm clearly correspond to the perpendicular to the metasurface plane and in-plane electric dipole resonances, respectively. The electric field at the wavelength of 2.80 μm is circulating, therefore this eigenmode correspond to the magnetic dipole resonance. The wavelengths of the eigenmodes are very close to the wavelengths of the resonances found in the previous simulations (Fig. 18).

5 Transmitarray design

Exciting both eigenmodes at a single wavelength, or, equivalently, overlapping both electric resonances in the bars enables full phase control of the transmitted fields. These resonances are excited at much closer wavelengths, therefore they are easier to tune. Besides of that, the origin of the resonances is the same, meaning that their properties change similarly with the wavelength.

Previously, in Fig. 19 the phase coverage of 2π with high transmission amplitude over a narrow range of frequencies was shown. Full phase control is essential for the realization of metasurfaces based on the conventional non-bianisotropic approach. Although bianisotropy gives a certain improvement, it is significant only at high angles. In this section a transmitarray working at the angle of 45° will be designed. In order to ease the designing process, non-bianisotropic inclusions will be utilized.

As it was mentioned previously, non-bianisotropic approach implies that the phase shift (Φ_t), generated by the inclusions, should be varied along the metasurface plane following the generalized Snell's law (Eq. (21)). Basically, this means that the phase should be gradually increasing from 0 to 2π in the range of one period. Although the amplitude of the transmitted field is not controlled, it should be high, in order to ensure solid performance of the metasurface. The supercell period is governed by the wavelength, which is 1.55 μm in the current design, and by the angles of incidence and transmission, which are 45° and 0°, respectively. By using these parameters in Eq. (22), the period of the supercell is calculated. The obtained value is 2190 nm. However, the size of inclusions is such that only three of them can fit in one period. It means that the phase gradient cannot be built smoothly in this case. As a result, the wavefront cannot be shaped perfectly, limiting the efficiency of the design.

The supercell of the structure, that will be presented further, contains three inclusions that can be designed separately. Placing each inclusion in a periodic array and tuning this array to give a certain phase (with a high amplitude) in transmission allows to design the inclusions. The inclusions can be tuned by varying the shape parameters of the resonators. In this particular case, the inclusions are dielectric bars

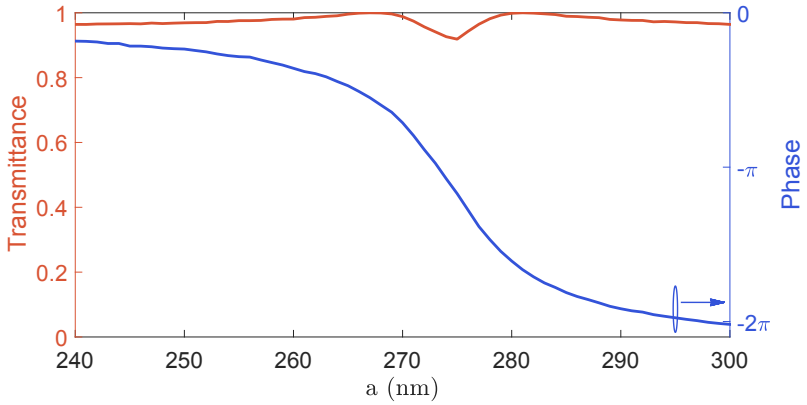

Figure 21: The transmission phase and amplitude for bars of different size. The refractive index of the dielectric is $n_{\mathrm{d}} = 6$.

with the width w and height h. Since the perpendicular electric dipole moment should be excited in the bars, an oblique illumination of the metasurface was considered. Figure 21 demonstrates the transmission amplitude and phase for arrays of bars with different shape parameters illuminated at an angle of $\theta_{\mathrm{i}} = 45°$. This graph was obtained by introducing a shape parameter a, such that the height and width of a bar depend on a as $h = a$ and $w = a + 10$ nm, respectively. The phase coverage of 2π with the transmission efficiency above 90% were achieved, by varying parameter a in the range between 240 nm and 300 nm. Worth noting that both the width and height of the bars were dependent on a, but it is possible to obtain higher or lower transmission with the same phase by varying these parameters separately. For this reason, after the transmitarray was formed, by choosing three suitable parameters a, it was optimized, considering the width w and height h as independent parameters. The efficiency of transmission of 84% was achieved in the simulations. Figure 22(a,b) demonstrates the electric field distributions in the far and near field regions of the transmitarray. The parameters of the structure are given in Fig. 22. In addition to that, all the bars in the structure are set equally distant from each other. Moreover, the bars in the simulations are centered, meaning that centers of the bars lay on one line. This is not very convenient from the practical point of view. Indeed, unlike metallic wires, the dielectric bars should be deposit the bars onto a substrate. In this case, not centers but bottoms of the bars are aligned. Simulating such structure

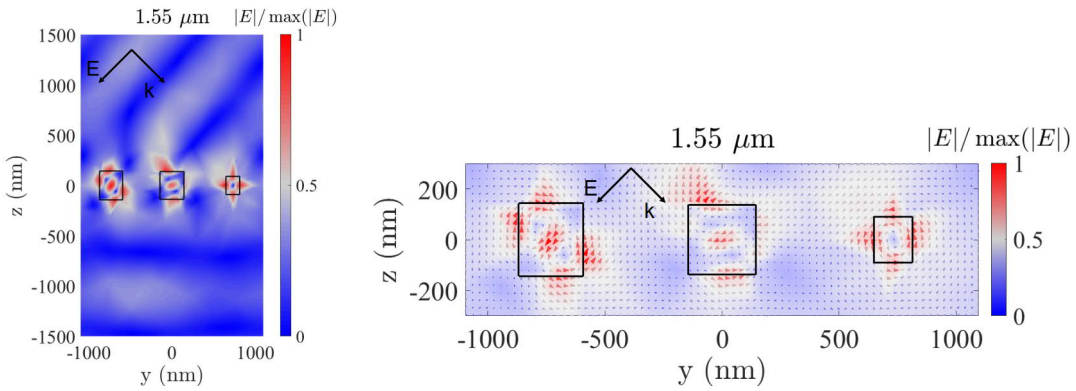

(a) (b)

Figure 22: Designed and optimized transmitarray. The width and height of the left bar - 276.7 nm and 286.8 nm, of the central - 288.4 nm and 275.2 nm, of the right - 164.8 nm and 180.7 nm. (a) and (b) The electric field distributions in the far field and near field regions, respectively.

without the substrate gave the same efficiency. The next step is to consider the substrate.

Basically, the presence of the substrate breaks the symmetry of the design, adding a bianisotropic response to the structure. From this point of view, asymmetry can increase the efficiency of the metasurface. However, due to different refractive indices of the substrate and vacuum, the wavelength in the substrate changes. As a result, the total number of propagating modes can increase. Coupling of some energy to these undesired modes needs to be nullified, which might be problematic.

Another important issue is available materials. As it was stated previously, for the explicit demonstration of the results, the bars are made of a dielectric material with the refractive index $n_{\mathrm{d}} = 6$. The metasurface, presented in Fig. 22, works at the wavelength of 1.55 μm. However, at this wavelength there are no low-loss materials with the refractive index $n_{\mathrm{d}} = 6$. Such materials exist only at the wavelength above 5 μm. Nevertheless, due to the linearity of Maxwell's equations, the designed structure can be scaled to work at the wavelength of 5 μm.

A widely used material at the wavelengths near 1.55 μm is silicon. The refractive

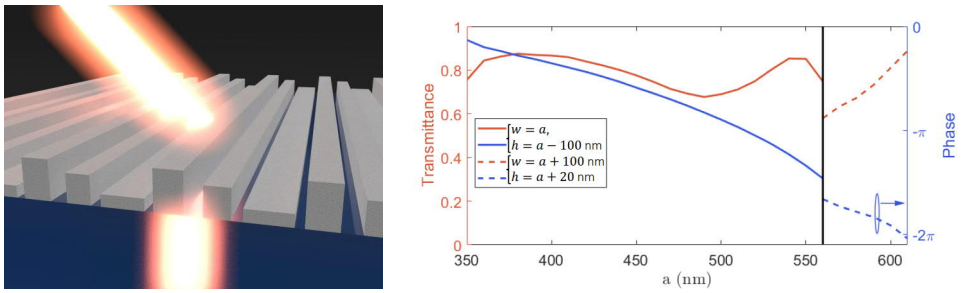

(a) (b)

Figure 23: The transmission and phase and amplitude for bars of different size. The refractive index of the dielectric is $n_{\mathrm{d}} = 3.48$.

index n_{d} of this material is $\sim$ 3.48 and it is practically lossless. Therefore, in order to design a real structure operating at the wavelengths of 1.55 μm, silicone can be used as a material for the bars. The electrical size of the bars should be approximately the same as it was for $n_{\mathrm{d}} = 6$. Since, now that the bars are made of less optically dense material, their physical dimensions will increase. Indeed, in order to obtain the phase coverage of 2π with high transmission amplitude the sizes of the bars made of silicon is varied from 250 nm to 700 nm. Although the full phase coverage is obtained by varying one size parameter a, the sizes of the bars depend on the parameter a differently in two regions (see Fig. 23). When values of a lie between 350 nm and 560 nm, the width and height of the bars depend on a as $w = a$ and $h = a - 100$ nm. When parameter a takes values in the range from 560 nm to 610 nm, the width and height are taken as $w = a + 100$ nm and $h = a + 20$ nm. It is worth to note that Fig. 23 is obtained by simulating an array of bars on a glass substrate with refractive index $n_{\mathrm{sub}} = 1.45$. Although in comparison to the previous case ($n_{\mathrm{d}} = 6$) lower values of transmission are obtained, these values can be changed by varying the size parameters independently. Therefore, final optimization of the structure is necessary for achieving highly efficient transmitarray.

The coupling between the bars can also be optimized, by changing the distance between the bars. It provides additional degrees of freedom, offering additional parameters for the optimization. For the structure presented in Fig. 24, even without

optimized coupling the efficiency of 88% was achieved in simulations. Optimizing the coupling might increase the efficiency, however, it was not done within this work. Figure 24 represents the electric field distribution in the transmitarray operating at the wavelength of 1.55 μm as well as the size parameters of the structure.

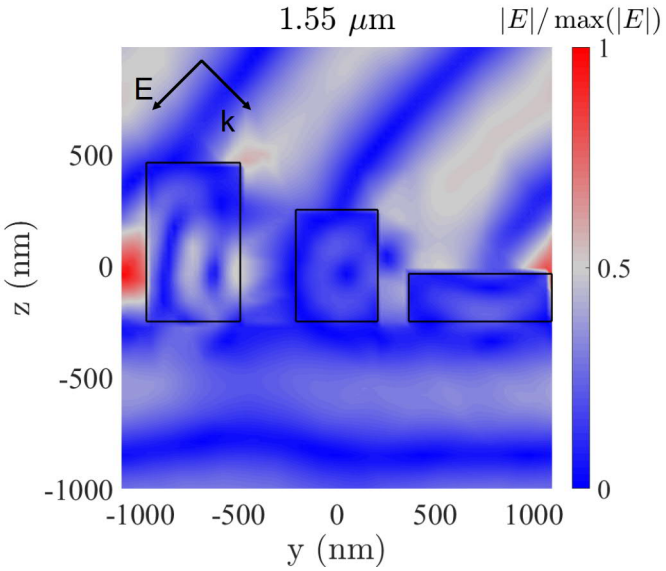

Figure 24: Designed and optimized transmitarray made of silicon bars ($n_{\mathrm{d}} = 3.48$) on a glass substrate ($n_{\mathrm{sub}} = 1.45$). The width and height of the left bar are 478 nm and 712 nm; of the central - 417 nm and 501 nm; of the right - 728 nm and 214 nm.

6 Discussion and conclusions

This thesis considers metasurfaces from various points of view. In the first part of the thesis we review approaches for characterization of metasurfaces. The first approach considers metasurfaces as planar layers, by using the generalized sheet transition conditions. In particular, these conditions were used in order to calculate the phase of the reflected field at the resonant wavelengths. The second approach from the review studies an equivalent representation of metasurfaces in form of three impedance layers, by using the circuit theory. In terms of this approach the conditions of ideal refraction are defined. In particular, utilization of this theory allowed us to compare the designs made of bianisotropic and non-bianisotropic inclusions. For transmitarrays operating at small angles ($\theta_{\mathrm{i}} < 45°$) the efficiency of non-bianisotropic designs is quite close to 100%, therefore, for simplicity non-bianisotropic approach was utilized for the transmitarrays designed in this work.

Examples of metasurfaces in optics, reviewed in this thesis, demonstrated realization of full phase control by spectrally overlapped the electric and magnetic resonances. However, this approach has disadvantages and its utilization might be problematic. Therefore, this thesis studies a new approach for obtaining full phase control in all-dielectric metasurfaces. The approach is based on the excitation of perpendicular eigenmodes of the metasurface, by using oblique incidence. Spectrally overlapping perpendicular and tangential eigenmodes also provides a phase coverage of 2π with high transmission amplitude. By using this approach a transmitarray was designed. The material for the bars with $n_{\mathrm{d}} = 6$ was used, in order to ease the design process. The light, incident on such metasurface at the angle of 45°, is transmitted normally with the efficiency of 84%. In order to design a real transmitarray working in optics, other materials were used. The real structure that can be fabricated consists of bars made of silicon with refractive index $n_{\mathrm{d}} = 3.48$ and a glass substrate ($n_{\mathrm{sub}} = 1.48$). Simulations of this structure resulted in even better efficiency: 88% of incident energy was transmitted into the desired direction.

In order to obtain better results, one could try to optimize the interaction between

the bars by varying the distance between them. However, the obtained increase of the efficiency will be a pure result of the optimization. The main goal of the thesis is to achieve full phase control by using only the electric response of the metasurface. Designed transmitarrays demonstrate the applicability of the novel approach.

In conclusion, the developed approach broadens the range of possibilities for metasurface designs. Excitation of the electric eigenmodes normal to the metasurface gives an additional degree of freedom in designing process. The geometry of metasurfaces suggested in the thesis can be replaced by another one. The only condition is nonzero thickness of the metasurface. It is needed in order to ensure existence of perpendicular eigenmodes in the metasurface. Worth to note that an oblique incidence is not obligatory in this approach. The designed transmitarrays are reciprocal, meaning that illuminating it from the substrate normally, the light will be refracted at the angle of 45°.

Any structure designed by following the suggested approach consists of inclusions of different heights. Although the fabrication of such structures might be problematic, it is not impossible. Future work includes fabrication of the structure, consisting of silicon bars on a glass substrate. Facilities of Micronova cleanrooms allows us to fabricate such structure.

The approach can also be extended to cover TE polarization of the incident light. In this case the normal magnetic mode will be excited instead of the electric one. Overlapping both tangential and perpendicular magnetic eigenmodes also provides full phase control. In this thesis it was not done, therefore it can be considered as a proposal for future work.

References

[1] S. Tretyakov, *Analytical modeling in applied Electromagnetics*. Artech House, 2003.

[2] A. Sihvola, "Metamaterials in electromagnetics," *Metamaterials*, vol. 1, no. 1, pp. 2–11, 2007.

[3] M. Albooyeh, S. Tretyakov, and C. Simovski, "Electromagnetic characterization of bianisotropic metasurfaces on refractive substrates: General theoretical framework," *Annalen der Physik*, vol. 528, no. 9-10, pp. 721–737, 2016.

[4] M. Idemen and A. Serbest, "Boundary conditions of the electromagnetic field," *Electronics Letters*, vol. 23, no. 13, pp. 704–705, 1987.

[5] M. Idemen, *Discontinueties in the Electromagnetic Field*. John Wiley & Sons, 2011.

[6] E. Kuester, M. Mohamed, M. Piket-May, and C. Holloway, "Averaged transition conditions for electromagnetic fields at a metafilm," *IEEE Transactions on Antennas and Propagation*, vol. 51, no. 10, pp. 2641–2651, 2003.

[7] V. S. Asadchy, M. Albooyeh, S. N. Tcvetkova, A. Díaz-Rubio, Y. Ra'di, and S. A. Tretyakov, "Perfect control of reflection and refraction using spatially dispersive metasurfaces," *Physical Review B*, vol. 94, no. 7, p. 075142, 2016.

[8] S. Larouche and D. R. Smith, "Reconciliation of generalized refraction with diffraction theory," *Optics Letters*, vol. 37, no. 12, pp. 2391–2393, 2012.

[9] N. Yu, P. Genevet, M. Kats, F. Aieta, J.-P. Tetienne, F. Capasso, and Z. Gaburro, "Light propagation with phase discontinuities: Generalized laws of reflection and refraction," *Science*, vol. 334, no. 6054, pp. 333–337, 2011.

[10] A. Epstein and G. Eleftheriades, "Huygens' metasurfaces via the equivalence principle: design and applications," *Journal of the Optical Society of America B*, vol. 33, no. 2, pp. A31–A50, 2016.

[11] J. B. Pendry, A. J. Holden, D. J. Robbins, and W. J. Stewart, "Magnetism from conductors and enhanced nonlinear phenomena," *IEEE Transactions on Microwave Theory and Techniques*, vol. 47, no. 11, pp. 2075–2084, 1999.

[12] R. Alaee, M. Albooyeh, M. Yazdi, N. Komjani, C. Simovski, F. Lederer, and C. Rockstuhl, "Magnetoelectric coupling in nonidentical plasmonic nanoparticles: Theory and applications," *Physical Review B*, vol. 91, no. 11, p. 115119, 2015.

[13] C. Pfeiffer and A. Grbic, "Metamaterial Huygens' surfaces: Tailoring wave fronts with reflectionless sheets," *Physical Review Letters*, vol. 110, p. 197401, May 2013.

[14] J. Wong, A. Epstein, and G. Eleftheriades, "Reflectionless wide-angle refracting metasurfaces," *IEEE Antennas and Wireless Propagation Letters*, vol. 15, pp. 1293–1296, 2016.

[15] J. Wong, M. Selvanayagam, and G. Eleftheriades, "Design of unit cells and demonstration of methods for synthesizing huygens metasurfaces," *Photonics and Nanostructures-Fundamentals and Applications*, vol. 12, no. 4, pp. 360–375, 2014.

[16] C. Pfeiffer and A. Grbic, "Millimeter-wave transmitarrays for wavefront and polarization control," *IEEE Transactions on Microwave Theory and Techniques*, vol. 61, no. 12, pp. 4407–4417, 2013.

[17] C. Pfeiffer and A. Grbic, "Bianisotropic metasurfaces for optimal polarization control: Analysis and synthesis," *Physical Review Applied*, vol. 2, no. 4, p. 044011, 2014.

[18] M. Chen, E. Abdo-Sánchez, A. Epstein, and G. Eleftheriades, "Experimental verification of reflectionless wide-angle refraction via a bianisotropic huygens' metasurface," *arXiv preprint arXiv:1703.06669*, 2017.

[19] C. Pfeiffer, N. Emani, A. Shaltout, A. Boltasseva, V. Shalaev, and A. Grbic, "Efficient light bending with isotropic metamaterial huygens' surfaces," *Nano Letters*, vol. 14, no. 5, pp. 2491–2497, 2014.

[20] V. Asadchy, Y. Ra'di, J. Vehmas, and S. Tretyakov, "Functional metamirrors using bianisotropic elements," *Physical Review Letters*, vol. 114, no. 9, p. 095503, 2015.

[21] A. Elsakka, V. Asadchy, I. Faniayeu, S. Tcvetkova, and S. Tretyakov, "Multifunctional cascaded metamaterials: Integrated transmitarrays," *IEEE Transactions on Antennas and Propagation*, vol. 64, no. 10, pp. 4266–4276, 2016.

[22] G. Lavigne, K. Achouri, V. Asadchy, S. Tretyakov, and C. Caloz, "Diffraction-free refracting metasurfaces," *arXiv preprint arXiv:1705.09286*, 2017.

[23] F. Monticone, N. Estakhri, and A. Alù, "Full control of nanoscale optical transmission with a composite metascreen," *Physical Review Letters*, vol. 110, no. 20, p. 203903, 2013.

[24] J. Zhou, T. Koschny, M. Kafesaki, E. Economou, J. Pendry, and C. Soukoulis, "Saturation of the magnetic response of split-ring resonators at optical frequencies," *Physical Review Letters*, vol. 95, no. 22, p. 223902, 2005.

[25] M. Decker, I. Staude, M. Falkner, J. Dominguez, D. Neshev, I. Brener, T. Pertsch, and Y. Kivshar, "High-efficiency dielectric Huygens' surfaces," *Advanced Optical Materials*, vol. 3, no. 6, pp. 813–820, 2015.

[26] Y. Yu, A. Zhu, R. Paniagua-Dominguez, Y. Fu, B. Luk'yanchuk, and A. Kuznetsov, "High-transmission dielectric metasurface with 2π phase control at visible wavelengths," *Laser and Photonics Review*, vol. 9, no. 4, pp. 412–418, 2015.

[27] M. Shalaev, J. Sun, A. Tsukernik, A. Pandey, K. Nikolskiy, and N. Litchinitser, "High-efficiency all-dielectric metasurfaces for ultracompact beam manipulation in transmission mode," *Nano Letters*, vol. 15, no. 9, pp. 6261–6266, 2015.

[28] V. Asadchy, M. Albooyeh, and S. Tretyakov, "Optical metamirror: all-dielectric frequency-selective mirror with fully controllable reflection phase," *Journal of the Optical Society of America B*, vol. 33, no. 2, pp. A16–A20, 2016.

[29] Y. Ra'di, V. Asadchy, and S. Tretyakov, "Tailoring reflections from thin composite metamirrors," *IEEE Transactions on Antennas and Propagation*, vol. 62, no. 7, pp. 3749–3760, 2014.